Journal of Infrastructure
Preservation and Resilience

RESEARCH **Open Access**

Classification of failure modes of pipelines containing longitudinal surface cracks using mechanics-based and machine learning models

Haotian Sun and Wenxing Zhou*

Abstract

This paper applies the mechanics-based approach and five machine learning algorithms to classify the failure mode (leak or rupture) of steel oil and gas pipelines containing longitudinally oriented surface cracks. The mechanics-based approach compares the nominal hoop stress remote from the surface crack at failure and the remote nominal hoop stress to cause unstable longitudinal propagation of the through-wall crack to predict the failure mode. The employed machine learning algorithms consist of three single learning algorithms, namely naïve Bayes, support vector machine and decision tree; and two ensemble learning algorithms, namely random forest and gradient boosting. The classification accuracy of the mechanics-based approach and machine learning algorithms is evaluated based on 250 full-scale burst tests of pipe specimens collected from the open literature. The analysis results reveal that the mechanics-based approach leads to highly biased classifications: many leaks erroneously classified as ruptures. The machine learning algorithms lead to markedly improved accuracy. The random forest and gradient boosting models result in the classification accuracy of over 95% for ruptures and leaks, with the accuracy of the decision tree and support vector machine models somewhat lower. This study demonstrates the value of employing machine learning models to improve the integrity management practice of oil and gas pipelines.

Keywords Pipeline, Crack, Failure mode, Machine learning models, Mechanics-based models, Full-scale test

Introduction

Buried steel pipelines are part of critical infrastructure systems in a modern society and widely recognized as the most efficient and safest means to transport crude oil, natural gas and other hydrocarbon products. The structural integrity of these pipelines is threatened by various failure mechanisms such as the third-party interference, corrosion, stress corrosion cracking and ground movement. Among them, cracking is one of the most serious failure mechanisms [16]. According to the data released by the Canadian Energy Pipeline Association [14, 15], cracking accounted for 15.8% and 13% of the total incidents on oil and gas transmission pipelines in Canada between 2010 and 2014 and 2016–2020, respectively. When an operating pipeline fails at a longitudinally oriented surface (i.e. part through-wall) crack due to internal pressure, the remaining ligament at the crack is severed, and the surface crack becomes a through-wall crack [2, 40]. Two failure modes of the crack are commonly recognized, namely leak and rupture [40, 61]. A failure is classified as a leak, also commonly referred to as a large leak in practice [52], if the longitudinal extension of the through-wall crack resulting from the failure of the surface crack is arrested or stabilized; it is defined as a rupture if unstable extension of the through-wall crack in the longitudinal direction takes place [69]. Ruptures of pipelines have much more severe consequences in terms of human safety and environmental impact than

*Correspondence:
Wenxing Zhou
wzhou@eng.uwo.ca
Department of Civil and Environmental Engineering, The University of Western Ontario, London, Ontario N6A 5B9, Canada

leaks [42, 52]. Based on incidents data corresponding to the onshore natural gas transmission pipelines in the United States between 2002 and 2013, Lam and Zhou [43] reported that the likelihoods of ignition were around 3% and 30% in leak and rupture incidents, respectively. They also found that 75% of fatalities and 83% of injuries were due to ruptures. Bubbico [11] performed a similar analysis using data collected by PHMSA between 2010 and 2015 and concluded that for underground natural gas pipelines, the likelihoods of ignition were 7.6% and 30.8% for leak and rupture incidents, respectively. Therefore, the accurate prediction of the potential failure mode at a surface crack has significant implications for quantifying the failure consequences.

Several full-scale burst tests were conducted by different researchers [2, 40, 59, 63] to investigate the failure modes of pipes containing surface cracks. Shannon [61] proposed that the leak and rupture failure modes be separated by comparing the nominal hoop stress remote from the surface crack at failure, σ_{hb}, and the remote nominal hoop stress to cause unstable longitudinal propagation of the through-wall crack, σ_{hr}. A rupture will occur if $\sigma_{hb} \geq \sigma_{hr}$; otherwise, a leak will occur. Note that the lengths of the surface crack and its resulting through-wall crack are assumed to be the same in this approach. However, equations for σ_{hb} and σ_{hr} proposed by Shannon [61] only take into account the flow stress but not fracture toughness of the pipe steel, and therefore may not be adequate for pipelines containing surface cracks.

Many models have been developed to evaluate the failure stress of pipelines containing surface and through-wall cracks, for example, the well-known Battelle (i.e. Ln-Sec) model [40] and modified Battelle model [38, 39], CorLAS model [34, 55], PAFFC [45], PRCI MAT-8 [4, 5], and failure assessment diagram-based approaches recommended in API 579 [3], BS 7910 [10] and R6 [24]. However, the employment of these models in Shannon's approach to separate failure modes has, to our best knowledge, not been reported in the literature. The most relevant work is perhaps reported by Kiefner et al. [40], which is the basis of Shannon's approach. Kiefner et al. conducted 140 experiments using full-scale pipe specimens, of which 92 and 48 specimens contain through-wall and surface cracks, respectively. For the 48 specimens with surface cracks, in addition to the actual failure stresses (i.e. σ_{hb}), their failure modes were also reported. The actual failure stresses were then compared with the predicted σ_{hr} for the 48 specimens, such that the predicted failure modes are compared with the actual failure modes of these specimens. Although a good agreement between the predicted and actual failure modes is reported in [40], this approach is inadequate for in-service pipelines because σ_{hb} and σ_{hr} cannot be measured and must be evaluated to predict the failure mode.

As an alternative to Shannon's mechanics-based approach, machine learning (ML) models are suitable tools to deal with the leak-rupture separation, which is a typical binary classification problem. ML algorithms have been widely applied to the classification tasks in the pipeline integrity management practice [56]. Zhou et al. [69] employed the logistic regression to predict the probability of rupture for corroded pipelines as a function of the depth and length of the corrosion defect. Carvalho et al. [13] applied the multi-layer perceptron neural network to signals from inspection tools based on the magnetic flux leakage technology to predict the presence of defects on pipelines and categorize the types of defect; Cruz et al. [21] employed the neural network model to signals from the ultrasonic inspection tools to perform the same prediction and classification, and Liu et al. [47] used the particle swarm optimization support vector machine (SVM) on eddy-current signals to classify the defects on pipelines. Zadkarami et al. [67, 68] applied the neural network model to the pipeline inlet pressure and outlet flow signals to categorize the leakage size and position into ten classes.

The objective of the present study is to apply both the mechanics-based approach and ML models to classify the failure modes of pipelines containing longitudinal surface cracks by considering the pipe geometric and material properties and dimensions of the crack. The main novelty of the study is two-fold. First, while many models to predict burst capacities of pipelines containing surface-breaking and through-wall cracks, respectively, have been developed as described in the previous paragraphs, the incorporation of these models in a mechanics-based framework to predict the failure mode of pipelines containing surface cracks has not been reported in the literature. The present study sheds light on the adequacy of the mechanics-based approach in terms of the failure mode determination. Second, we develop machine learning models to predict the failure mode of pipelines containing surface cracks and compare the accuracy of the mechanics-based approach and machine learning models. To the best of our knowledge, similar investigations are unavailable in the literature. A database of full-scale burst tests involving pipe specimens containing surface cracks is collected from the open literature as the basis for training the ML models and also comparing the predictive accuracy of the mechanics-based approach and ML models. For the mechanics-based approach, the well-known CorLAS model ([55, 64, 66]) is selected to evaluate σ_{hb}, whereas the Battelle model and an extension of the CorLAS model for through-wall cracks [55] are used to evaluate σ_{hr}. Five ML models are considered for comparison with the mechanics-based approach, namely the naïve Bayes (NB) model, SVM, decision tree (DT), random forest (RF) and gradient boosting (GB).

The rest of the paper is organized as follows. Section "Mechanics-based models for failure mode classification" describes the two main components of the mechanics-based approach for classifying the failure mode, i.e. the models for calculating σ_{hb} and σ_{hr}, and illustrates the application of the mechanics-based approach on a hypothetical example; Section "Machine learning classification algorithms" describes the five ML models that are employed to classify the failure mode; Section "Full-scale burst tests of pipes containing longitudinal surface cracks" presents the details of the full-scale burst test data collected from the open literature and employed in the present study; Section "Classification results using mechanics-based models" introduces the metrics for evaluating the predictive performance of a classifier and presents the predictive performance of the mechanics-based approach applied to the full-scale test dataset described in Section "Full-scale burst tests of pipes containing longitudinal surface cracks"; the training and optimization of the five ML models and their predictive performances based on the full-scale test dataset are discussed in Section "Machine learning models for failure mode classification", followed by conclusions in Section "Conclusion".

Mechanics-based models for failure mode classification

Burst capacity model for surface cracks

Various burst capacity models have been proposed and employed in the industry for pipelines containing longitudinally oriented surface cracks over the past several decades, as described in the previous section. These models can generally be grouped into two categories, namely the pipeline-specific and generic crack assessment methods that are based on the failure assessment diagram concept [19]. Performances of some of the burst capacity models mentioned in Introduction have been evaluated and compared in the literature, e.g. Rothwell and Coote [60], Yan et al. [65], Yan et al. [64] and Guo et al. [28]. It has been consistently shown that the CorLAS model, the model built in the CorLAS™ software [22] that is well known in the pipeline industry [3, 54], is one of the most accurate burst capacity models for pipelines with longitudinal surface cracks. Therefore, the CorLAS model is employed in the present study to evaluate σ_{hb}. For clarity, this model is referred to as the CorLAS-S model (i.e. CorLAS model for surface cracks) to be distinguished from the CorLAS-based model for through-wall cracks as described in Section "Burst capacity models for through-wall cracks".

The CorLAS-S model was originally proposed by Jaske and Beavers [33] to predict burst capacities of pipelines containing longitudinal crack-like surface breaking flaws based on elastic-plastic fracture mechanics principles. The model has been continuously updated since then and is now in Version 3 [34, 55] with main formulations given by,

$$\sigma_{hb} = \sigma_{crit}\left(\frac{1-\frac{A}{A_0}}{1-\frac{A}{A_0 M}}\right) = \sigma_{crit}\left(\frac{1-\frac{\pi a}{4w_t}}{1-\frac{\pi a}{4w_t M}}\right) \tag{1}$$

$$\sigma_{crit} = \min\left\{\sigma_{ff}, \sigma_{ft}\right\} \tag{2}$$

$$\sigma_{ft} = \begin{cases} \sigma_l \;\; External \\ \left(\frac{2D}{2D+\pi a}\right)\sigma_l \;\; Internal \end{cases} \tag{3}$$

$$M = \begin{cases} \sqrt{1+0.6275\frac{(2c)^2}{Dw_t}-0.003375\frac{(2c)^4}{(Dw_t)^2}} & \frac{(2c)^2}{Dw_t} \le 50 \\ 3.3+0.032\frac{(2c)^2}{Dw_t} & \frac{(2c)^2}{Dw_t} > 50 \end{cases} \tag{4}$$

where A is the area of the longitudinal profile of the surface crack with a length $2c$ and a maximum depth a, as illustrated in Fig. 1; A_0 is the reference area that equals $2cw_t$ with w_t denoting the pipe wall thickness; M is the Folias factor that accounts for the defect bulging induced stresses due to pipe internal pressure [26], and D is the pipe outside diameter. It is emphasized that the CorLAS-S model assumes the crack profile to be semi-elliptical if a detailed crack profile is unavailable. Therefore, cracks with other profiles (e.g. rectangular) need to be converted into equivalent semi-elliptical profiles. Such a conversion is typically carried out by maintaining the same area and depth of the crack profile while obtaining an equivalent crack length [28, 35, 40]. For example, a rectangular crack with a length $2c_{rec}$ will have an equivalent semi-elliptical crack length $2c = (2c_{rec})(4/\pi)$ based on the above criterion.

As shown in Eq. (2), cracks are evaluated using the flow strength- (i.e. σ_{ff}) and fracture toughness-based (i.e. σ_{ft}) criteria in the CorLAS-S model. The criterion that leads to the lower failure stress is used to evaluate σ_{hb}. As such, σ_{ff} is defined as $(\sigma_y + \sigma_u)/2$, where σ_y and σ_u denote the yield strength and tensile strength of the pipe steel, respectively. The quantity σ_{ft} is directly related to the local failure stress, σ_l (Eq. (3)). If the crack is on the pipe external surface, $\sigma_{ft} = \sigma_l$, whereas an adjustment is needed for cracks on the pipe internal surface to account for the effect of internal pressure on the crack surface. The value of σ_l is obtained by

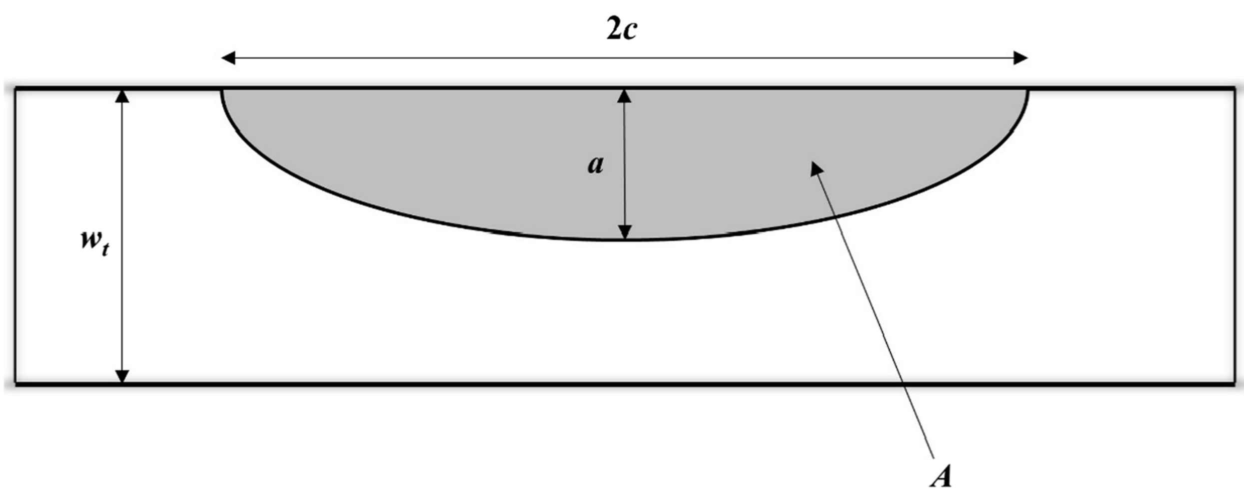

Fig. 1 Longitudinal profile of a semi-elliptical surface crack

solving for the stress satisfying $J_t = J_c$, where J_t and J_c are the total applied J-integral at the crack tip and fracture toughness of the pipe steel, respectively. If direct measurements of the fracture toughness of the pipe steel are unavailable, the following empirical equation can be used to estimate J_c from the Charpy V-notch (CVN) impact test result [35]:

$$J_c = \frac{C_v}{A_c} \tag{5}$$

where C_v and A_c denote the CVN impact energy and net cross-sectional area of the Charpy impact specimen, respectively. Detailed equations for calculating J_t are given in Appendix A.

Burst capacity models for through-wall cracks

Kiefner et al. [40] proposed the following semi-empirical model, also known as the Ln-Sec or Battelle model, to compute σ_{hr} based on the plastic-zone correction solution for cracks in flat plates with an infinite width [23]:

$$\frac{\pi K_c^2}{8c\sigma_f^2} = \ln\left\{\sec\left(\frac{\pi}{2}\frac{M\sigma_{hr}}{\sigma_f}\right)\right\} \tag{6}$$

where K_c denotes the fracture toughness of the pipe steel in terms of the stress intensity factor; σ_f represents the flow stress of the pipe steel, and all other variables have been defined previously. Note that $\sigma_f = \sigma_y + 68.95$ MPa, which is different from σ_{ff} in the CorLAS-S model. Since K_c may not be available in practice, it can be evaluated by the following empirical equation that is equivalent to Eq. (5) [50]:

$$K_c = \sqrt{\frac{C_v E}{A_c}} \tag{7}$$

where E denotes the modulus of elasticity of the pipe steel. Kawaguchi et al. [36] pointed out that Eq. (7) tends to be non-conservative for pipe steels with C_v greater than 130 J and grades higher than X65 and introduced a static Charpy test to improve the accuracy [37]. However, it is unclear if the static Charpy test has been adopted in practice.

Polasik et al. [55] modified the CorLAS model to apply it to through-wall cracks. This is referred to as the CorLAS-T model in the present study. According to this model, σ_{hr} can be evaluated by solving for the stress satisfying $J_{tT} = J_c$, where J_{tT} is the total applied J-integral at the tip of the through-wall crack (see Appendix A). Both the Battelle and CorLAS-T models are employed in the present study to calculate σ_{hr}.

Illustration of mechanics-based approach for failure mode classification

The application of the mechanics-based approach to predict the failure mode is illustrated using a hypothetical example. Consider a pipeline with $D = 610$ mm, $w_t = 7.2$ mm, $\sigma_y = 414$ MPa and $\sigma_u = 517$ MPa (i.e. X60 steel grade) that contains a single semi-elliptical crack. Figure 2 depicts the failure mode predicted by the mechanics-based approach for various crack lengths and depths, and three representative full-size CVN values ($C_v = 25$, 50 and 100 J). The solid lines in Fig. 2 correspond to σ_{hb} predicted by the CorLAS-S model for surface cracks with different depths and lengths, and the two dashed lines correspond to σ_{hr} predicted by the Battelle and CorLAS-T models, respectively, for

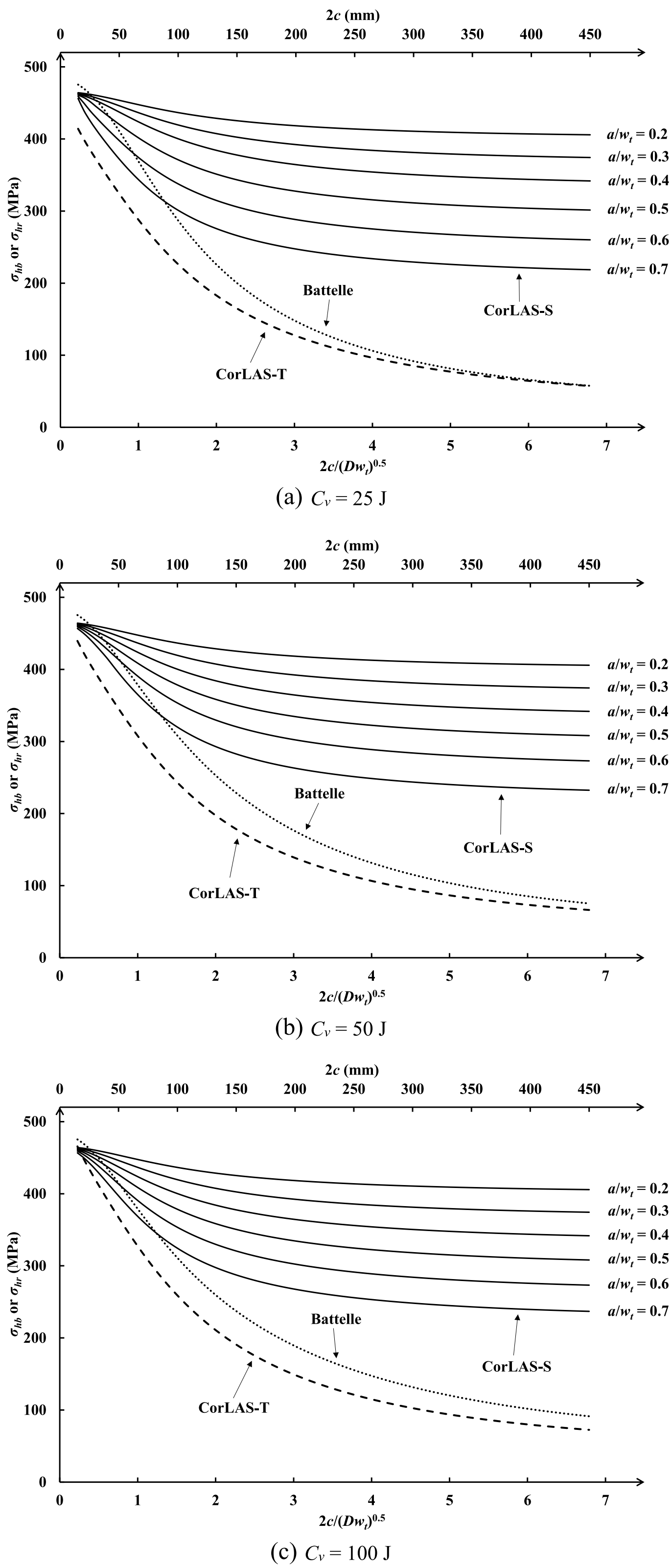

Fig. 2 Relationship between σ_{hb} and σ_{hr} with varying crack lengths and depths for a hypothetic pipeline example. **a** $C_v = 25$ J. **b** $C_v = 50$ J. **c** $C_v = 100$ J

through-wall cracks with different lengths. The figure indicates that the CorLAS-T model predicts consistently lower σ_{hr} values than the Battelle model. Suppose that the Battelle model is used to predict σ_{hr}. For surface cracks with a given depth, a rupture is predicted if the solid line corresponding to the crack depth is above the dashed line associated with the Battelle model; otherwise, a leak is predicted. The interception point between the solid and dashed lines defines the critical crack length; that is, rupture (leak) occurs if the crack length is greater than or equal to (less than) the critical length. Since the critical crack length decreases as the crack depth decreases, it follows that rupture (leak) is the more likely failure mode for shallow (deep) cracks. If the CorLAS-T model is used to predict σ_{hr}, Fig. 2 indicates that almost all of the considered surface cracks will be predicted to fail by rupture as the solid lines are all above the dashed line corresponding to CorLAS-T except for cases with very short cracks and $C_v = 100$ J. For this particular example, increasing C_v from 25 to 100 J has no impact on σ_{hb} corresponding to $a/w_t = 0.2$, 0.3 and 0.4 as the flow stress-based criterion governs the prediction of the CorLAS-S model. The increase in C_v leads to increased values of σ_{hb} corresponding to $a/w_t = 0.5$, 0.6 and 0.7 as the toughness-based criterion governs the prediction of the CorLAS-S model for these cases.

Machine learning classification algorithms

General

There are a great number of machine learning (ML) tools for classification tasks such as neural network and support vector machine (SVM). The ensemble methods, which utilize multiple learning algorithms in one ML model to achieve better predictive performance than using a single learning algorithm, have attracted much attention in the application of machine learning models [56]. Representative ensemble learning algorithms include the adaptive boosting, gradient boosting (GB), random forest (RF) and extremely randomized trees [25, 49, 56]. In the present study, three commonly used single ML algorithms for classification, namely naïve Bayes (NB), SVM and decision tree (DT), and two ensemble classification algorithms, namely RF and GB, are employed to predict the failure modes of the full-scale test data. The three single algorithms are selected because their underlying mechanisms for classification are completely different. RF and GB are selected as they are classic DT-based ensemble ML algorithms and respectively involve bagging and boosting so that the performances of the ensemble methods and conventional DT can be compared. The five selected ML algorithms are described briefly in the following sections.

Naïve Bayes

NB is a simple ML algorithm that utilizes Bayes' theorem for classification. The term "naïve" indicates the assumption that the input features associated with the data are mutually independent conditional on the class variable. For a given sample with a class variable y and m input features (x_1, x_2, …, x_m), NB is applied as follows:

$$P(y|x_1,\ldots,x_m) = \frac{P(y)\prod_{i=1}^{m}P(x_i|y)}{P(x_1,\ldots,x_m)} \propto P(y)\prod_{i=1}^{m}P(x_i|y) \tag{8}$$

$$\hat{y} = \mathrm{argmax}_y\left[P(y)\prod_{i=1}^{m}P(x_i|y)\right] \tag{9}$$

where $P(y)$ is the prior probability of class y; $P(x_i|y)$ is the likelihood of input feature x_i ($i = 1, 2, \ldots, m$) given class y; "$\propto$" denotes proportionality, and $\hat{y}$ is the prediction given by NB. $P(y)$ is usually set to be the frequency of the corresponding class variable in the training dataset. For continuous input features, $P(x_i|y)$ is typically evaluated based on the Gaussian assumption [51].

Support vector machine

SVM was originally developed for the binary classification [18] and subsequently extrapolated to the multiclass classification and regression. Consider that a training dataset consists of n samples, each with m input features and one of the two class variables, such that any sample can be represented as $\{\boldsymbol{x_j}, y_j\}$ ($j = 1, 2, \ldots, n$), where $\boldsymbol{x_j} \in R^m$ is an m-dimensional vector representing the input features of the sample, and $y_j \in \{-1, +1\}$ is the class label of the sample. The basic idea of the binary classification SVM is to nonlinearly map input vectors into a higher dimensional feature space, where a linear decision hyperplane can be constructed to separate the two classes, simultaneously maximizing the distance between them [18]. However, a rigorous linear separation of read-world data is usually infeasible, resulting in unavoidable misclassifications. Therefore, a strictly positive regularization parameter (C) that determines a trade-off between the number of misclassifications in the training dataset and the distance between two classes is an important hyper-parameter of SVM. Another significant hyper-parameter is the kernel function K, which defines the nonlinear mapping of the input vector into the high dimensional feature space. The commonly used Gaussian (i.e. radial basis function or RBF) kernel is given by Eq. (10),

$$K(\boldsymbol{x_j},\boldsymbol{x_k}) = e^{-\frac{\|\boldsymbol{x_j}-\boldsymbol{x_k}\|^2}{\gamma_G}} \tag{10}$$

where γ_G is the parameter of the Gaussian kernel. SVM has two advantages compared with other classification algorithms: it is not data-greedy and can well resist the effects of outliers [12].

Decision tree

DT can be used to deal with both classification and regression tasks. Therefore, DT is also referred to as the classification and regression tree (CART) [9]. A DT is built by splitting nodes of the tree structure into two child nodes recursively. The nodes that are split in a DT are decision nodes while those cannot be further split are called leaf nodes or leaves. The decision node located at the top of the (inverted) tree is the root node. From the root node, a DT grows as follows. First, given the training dataset with different input features, select the best split of each feature that optimizes the splitting criterion. Second, select the best split of the decision node among the best splits of features that optimizes the splitting criterion. Finally, split the decision node using the best split and repeat the process until a pre-determined stopping criterion is satisfied. A commonly used splitting criterion for classification trees is the Gini impurity index (GI), which is a measure of the total variance across all classes [32] and minimized to find the best split of a decision node. A natural stopping criterion for classification trees is that all leaves are pure, namely, each leaf node consisting of samples of the same class. Other stopping criteria such as limits on the levels of the tree or on the number of decision nodes could also be used. Compared with other ML algorithms, DT is simple, understandable and interpretable [32]. Furthermore, DT is a white box model [48] since its prediction is highly explainable as the movement of the sample through the tree can be directly visualized. However, DT is susceptible to overfitting [7], which may lead to a lack of robustness in the prediction and a more tedious hyper-parameter tuning process.

Random forest

RF [8] is a DT-based ensemble ML algorithm that involves bootstrap aggregating (known as bagging). An RF consists of a large number of DTs, and the split of every decision node in each DT is based on a randomly selected subset of the input features, unlike conventional DT, which considers all input features. To train an RF, numerous subsets of data are first randomly sampled with replacement (i.e. bootstrap sampling) from the training dataset. Each bootstrapped subset of data is then used to generate a DT. When this RF is applied to a new sample, each DT in the forest provides a prediction of the class of the sample. The class predicted by the majority of the trees in the RF is the final prediction, i.e. aggregating. Compared with DT, RF is capable of handling numerous input features, more robust to deal with outliers, and less susceptible to overfitting. However, the interpretability of the algorithm is simultaneously sacrificed due to numerous DTs in the forest. RF also inherently evaluates the importance of each input feature, which will be described in Section "Machine learning models for failure mode classification".

Gradient boosting

GB was first proposed for regression and subsequently extrapolated for classification [27]. It establishes a forward stepwise additive structure that amalgamates the predictions given by several sequential weak learners, which are typically DTs [29]. Unlike RF, the weak learners in GB are regression trees even if GB is used for classification. Given the training dataset, the goal is to develop a model that maps the input features to the corresponding class variable for each sample in the dataset by minimizing a loss function, which is typically the log-likelihood (also known as deviance) in GB for classification. The procedure is iterative in that the model is continuously and sequentially revised by adding regression trees to fit the residual of the model prediction at the previous step of iteration so that the value of the loss function continuously decreases. A critical hyper-parameter of GB is the learning rate. It scales the step length in search for the minimum value of the loss function and also limits the contribution of each regression tree. The numerical prediction given by the additive regression trees is transferred to a probability measure through the logistic function, which quantifies the probability of the sample belonging to the positive class to achieve classification. More details of GB can be found in [29].

Full-scale burst tests of pipes containing longitudinal surface cracks

A total of 250 full-scale tests of pipe specimens containing single longitudinal surface cracks are collected from the literature [2, 20, 31, 36, 40, 57–59, 63]. The test data include 135 leaks and 115 ruptures. All 250 data points have D/w_t values greater than or equal to 20 except the eight test specimens reported in [63], the D/w_t of which equal 19.50 and 19.95. Therefore, all specimens are considered thin-walled. The yield and tensile strengths as well as C_v of each pipe specimen are provided in the corresponding source documents. The crack profiles in the dataset are either rectangular or semi-elliptical. Five specimens in [63] have cracks on the internal pipe surface; nineteen specimens, also reported in [63], have no information as to whether the cracks are internal or external. All the other specimens have external cracks. In the subsequent analyses, cracks with unknown positions (internal or external) are assumed to be external cracks as such information is required for the evaluation of σ_{hb} (see

Eqs. (1) to (3)). However, it is noted that the crack position has a marginal impact on σ_{hb}. A brief summary of the geometric and material properties of the pipe specimens in the test database collected is given in Table 1. Details of the test data are provided in Appendix B.

Classification results using mechanics-based models

Evaluation metrics of classifier performance

For binary classification problems, one can define any of the two classes to be positive and the other negative. Depending on whether a classifier correctly or incorrectly identifies the positive and negative classes, there are four possible outcomes of the prediction by the classifier, namely true positive (TP), true negative (TN), false positive (FP) and false negative (FN). FP and FN are also known as type-I and type-II errors, respectively [1]. Given these four possible outcomes, some commonly used evaluation metrics of the performance of a classifier are described as follows. Let n_{TP}, n_{TN}, n_{FP}, n_{FN} respectively denote the numbers of TP, TN, FP and FN after a classifier has been applied to a dataset. The true positive rate (TPR), i.e. sensitivity, and true negative rate (TNR), i.e. specificity, are defined as follows [1]:

$$\mathrm{TPR} = \frac{n_{TP}}{n_{TP} + n_{FN}} \tag{11}$$

$$\mathrm{TNR} = \frac{n_{TN}}{n_{TN} + n_{FP}} \tag{12}$$

Another commonly used metric is the accuracy (ACU), which represents the total percentage of correctly predicted classes:

$$\mathrm{ACU} = \frac{n_{TP} + n_{TN}}{n_{tot}} \tag{13}$$

where $n_{tot} = n_{TP} + n_{FN} + n_{TN} + n_{FP}$ is the total number of samples in the dataset. More sophisticated evaluation metrics such as the F-score and Matthews correlation coefficient have been proposed [17] but are not employed in the present study as the above-described simple evaluation metrics are considered sufficient to quantify the performances of the binary classifiers.

Predictions of the mechanics-based approach based on test data

The three models described in Section "Mechanics-based models for failure mode classification", i.e. CorLAS-S, CorLAS-T and Battelle models, are applied to the full-scale test dataset described in Section "Full-scale burst tests of pipes containing longitudinal surface cracks" to predict the failure mode of each test specimen. Two scenarios are considered in the analysis: scenario #1 involving using the CorLAS-S and Battelle models to predict σ_{hb} and σ_{hr}, respectively, and scenario #2 involving using the CorLAS-S and CorLAS-T models to predict σ_{hb} and σ_{hr}, respectively. Prior to the calculation of the CorLAS-S model, cracks having rectangular profiles are converted to equivalent semi-elliptical profiles by maintaining the same profile area and maximum depth but evaluating the equivalent crack length. On the other hand, actual crack lengths are employed in the CorLAS-T and Battelle models, regardless of the crack profile. The failure modes of 228 tests (126 leaks and 102 ruptures) out of a total 250 tests are predicted. The prediction is not obtained for 22 tests for the following reasons. The CorLAS-S model is inapplicable to three tests in [40] because the ultimate tensile strengths of the specimens are not provided. Solutions of σ_{hb} were not obtained due to numerical difficulties when the CorLAS-S model was applied to the six tests reported in [57] and thirteen tests reported in [58]. The predictive performance of the mechanics-based approach corresponding to the two scenarios is presented in Fig. 3 and Table 2. Figure 3 includes the evaluation metrics described in Eqs. (11) to (13), and Table 2 displays the confusion matrix, which is constituted by the four possible types of outcomes of a classifier. Rupture and leak are designated as the positive and negative classes, respectively, in the present study. The bracketed number in the confusion matrices represents the total number of a particular failure mode based on the actual full-scale test data or model predictions.

As indicated in Fig. 3, under both scenarios, the mechanics-based approach results in sensitivity values of over 96% and specificity values of between 20 and 30%. This indicates that the mechanics-based approach is highly accurate in identifying ruptures but has a poor

Table 1 Ranges of geometric and material properties of 250 burst tests data

	D (mm)	w_t (mm)	*a* (mm)	2*c* (mm)	D/w_t	a/w_t	σ_y (MPa)	σ_u (MPa)	C_v (J)[a]
Min.	76.40	3.20	0.80	17.00	19.50	0.19	246.00	454.00	19.20
Max.	1422.40	21.70	17.80	609.60	103.96	0.99	1096.27	1179.00	261.00
Mean	368.08	8.24	5.77	122.27	40.93	0.71	654.45	794.87	77.36
COV (%)[b]	82.2	54.6	57.7	91.2	53.2	21.4	37.5	26.7	69.4

[a] Full-sized CVN test specimen

[b] Coefficient of variation

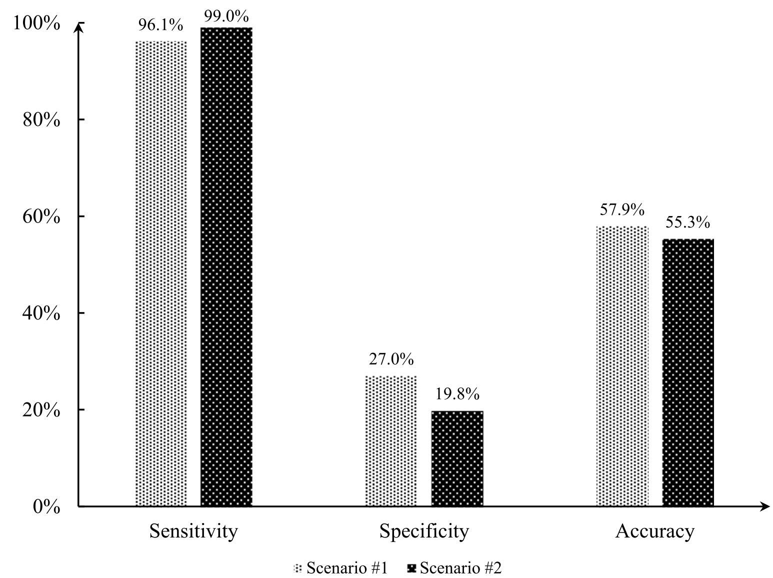

Fig. 3 Classification performance of the physics-based approach on 228 data points

Table 2 Confusion matrix of the physics-based approach on 228 data points

(a) Scenario #1			
Total number of samples = 228		Predicted failure mode	
		Rupture (190)	Leak (38)
Actual failure mode	Rupture (102)	$n_{TP}=98$	$n_{FN}=4$
	Leak (126)	$n_{FP}=92$	$n_{TN}=34$
(b) Scenario #2			
Total number of samples = 228		Predicted failure mode	
		Rupture (202)	Leak (26)
Actual failure mode	Rupture (102)	$n_{TP}=101$	$n_{FN}=1$
	Leak (126)	$n_{FP}=101$	$n_{TN}=25$

accuracy in identifying leaks. The overall accuracy of the mechanics-based approach is about 55%. Scenario #1 corresponds to a slightly better predictive performance than scenario #2 as the former achieves a higher accuracy and greater balance between the sensitivity and specificity. A possible explanation for the poor accuracy of the mechanics-based approach in identifying leaks is that the CorLAS-S model is relatively accurate in evaluating σ_{hb} but the Battelle and CorLAS-T models both markedly underestimate σ_{hr}. It follows from the above results that the ML approach is needed to classify ruptures and leaks more accurately.

Machine learning models for failure mode classification

Selection of input features

Based on the results presented in Section "Illustration of mechanics-based approach for failure mode classification", the normalized crack depth and length, a/w_t and $2c/(Dw_t)^{0.5}$, are selected as the input features for the ML models. It must be emphasized that a and $2c$ are assumed to be the depth and length of a semi-elliptical crack profile; therefore, a non-semi-elliptical crack profile should be converted to an equivalent semi-elliptical profile (see Section "Burst capacity model for surface cracks"). In addition to a/w_t and $2c/(Dw_t)^{0.5}$, two pipe material properties, i.e. σ_y and C_v, are compounded into a non-dimensional input feature that quantifies the relative resistance to two competing failure mechanisms, i.e. plastic collapse and fracture, of the remaining ligament at the crack, i.e. $A_c\ (w_t\text{-}a)\sigma_y/C_v$ [30]. Note that $(w_t\text{-}a)\ \sigma_y$ and C_v/A_c in this compound parameter respectively quantify the resistance of the remaining ligament to plastic collapse and fracture. Figure 4 depicts the failure modes versus any two of the three input features for the 250 test data described in Section "Full-scale burst tests of pipes containing longitudinal surface cracks". Figure 4(a) indicates that leaks tend to occur at deep cracks, which is consistent with the predictions by the mechanics-based approach. However, the correlation between the normalized crack length and failure mode is unclear. Figures 4(b) and (c) suggest that leaks are more likely for pipe specimens with low values of $A_c\ (w_t\text{-}a)\sigma_y/C_v$. This confirms the relevance of the input feature $A_c\ (w_t\text{-}a)\sigma_y/C_v$.

Model development

The full dataset is randomly divided into 80% and 20% portions, i.e. 200 and 50 data points, as the training and test datasets, respectively. The stratified sampling is employed to generate the training and test datasets; that is, the 80%–20% separation is applied to ruptures and leaks to avoid bias in the two subsets. As such, the training dataset consists of 108 leaks and 92 ruptures, while the test dataset consists of 27 leaks and 23 ruptures.

The five ML algorithms as described in Section "Machine learning classification algorithms" are then respectively applied to the training dataset to establish classifiers. The ten-fold cross validation combined with randomized search [6, 29] is employed to conduct the hyper-parameter tuning for the five algorithms. The value of each hyper-parameter is first randomly selected from a pre-defined range such that a set of values of the hyper-parameters is used to conduct the ten-fold cross validation. We then equally divide the training dataset into ten subsets, employ any nine subsets to train a model with the given set of hyper-parameters and apply the model to the remaining subset to evaluate the model performance. Such a process is repeated ten times such that each subset has been used exactly once for the validation. Model performances on all ten subsets can then be averaged as the final performance of the model corresponding to the given set of hyper-parameters. The set of hyper-parameters that results in the best model performance in the cross validation is then selected as the tuned hyper-parameters. Note that the stratified sampling is also applied to generate each of the ten subsets of the training dataset for the ten-fold cross validation. The predictive performance criterion employed in the cross validation is the accuracy (ACU) as defined in Eq. (13). With a relatively balanced dataset in which the negative class (i.e. leak) accounts for 54%, ACU provides an adequate measure of the predictive accuracy associate with rupture and leak. It is also the most commonly used evaluation metric for classification analysis in pipeline integrity management as indicated in [56].

The ML models in the present study are developed utilizing specialized packages *pandas* and *scikit-learn* [53] in the open-source platform *Python*. The values of the tuned hyper-parameters of the five algorithms are summarized in Table 3. Other hyper-parameters take the default values embedded in *scikit-learn*. The prior probabilities of both classes ("priors") in NB are tuned, as the proportions of ruptures and leaks in the training dataset do not necessarily represent those in reality. The Gaussian NB is employed since all three input features are continuous variables. The Gaussian kernel is employed in SVM, and the regularization parameter (C) and kernel coefficient (γ_G) as described in Section "Support vector machine" are tuned. The tuned hyper-parameters of DT include the maximum number of levels in the tree (max_depth), minimum number of samples required to split a decision node (min_samples_split) and minimum number of samples required in each leaf node (min_samples_leaf). The three tuned hyper-parameters for DT are also employed in RF. In addition, two other hyper-parameters of RF are tuned: the number of trees in the forest (n_estimators) and number of input features to consider for the best split (max_features). The tuned hyper-parameters in GB are the same as those in RF except that max_features is replaced by the learning rate (learning_rate) since all input features are considered at every split of the regression trees in each iteration in GB. The search spaces of all hyper-parameters included in Table 3 that are employed during the hyper-parameter tuning process are provided in Appendix C.

[a]The prior probabilities of leak and rupture, respectively.

Model performance evaluation

The five ML models developed based on the entire training dataset and tuned hyper-parameters are applied to the test dataset to predict the corresponding failure modes. The sensitivity, specificity and accuracy (see Section "Evaluation metrics of classifier performance") of the predictions given by each ML model on both the training and test datasets are summarized in Fig. 5. The confusion matrices of model predictions for the test dataset are shown in Table 4.

Figure 5 and Table 4 indicate that the five ML models lead to moderately accurate to highly accurate predictions of the failure modes. The predictions by the ML models are more balanced than those by the mechanics-based approach as predictions by the latter have a very low specificity. Among the three single ML algorithms, the Naïve Bayes (NB) performs markedly poorer than the support vector machine (SVM) and the decision tree (DT): NB has an accuracy of around 80% while the other two more than 90%. This could be attributed to that the Gaussian likelihood in NB may not be adequate for the input features. The predictive accuracy of DT is slightly better than SVM. The accuracies of the two ensemble algorithms, i.e. the random forest (RF) and the gradient boosting (GB), are above 95% and somewhat higher than that of DT. The results suggest that the SVM, DT, RF and GB models are highly effective in identifying the failure modes for pipelines containing longitudinal surface cracks. Furthermore, the ensemble ML algorithms are more advantageous than the single ML algorithms.

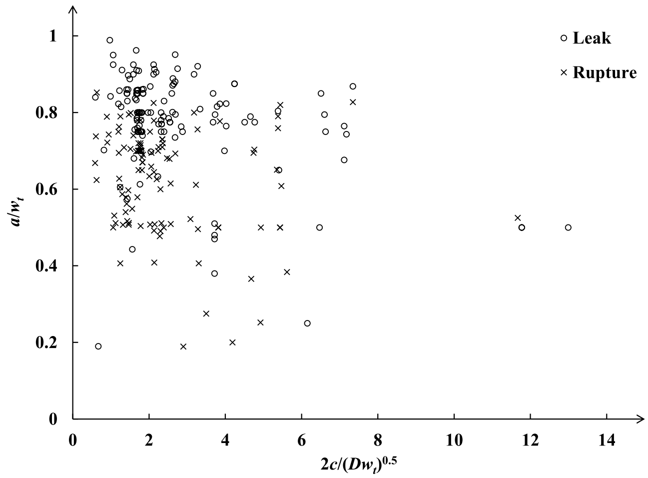

(a) Failure mode vs. a/w_t and $2c/(Dw_t)^{0.5}$

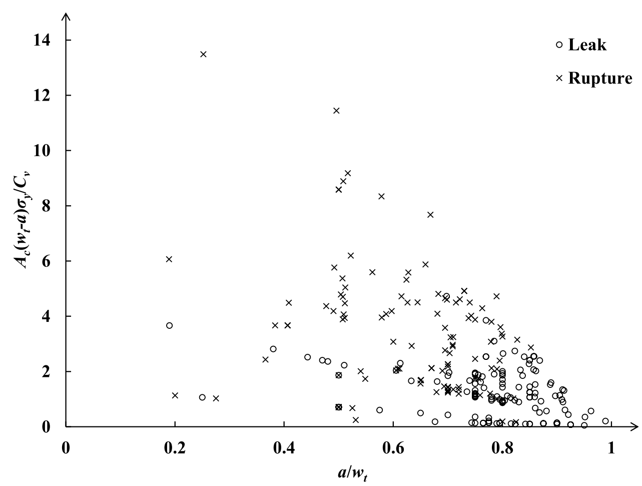

(b) Failure mode vs. $A_c(w_t\text{-}a)\sigma_y/C_v$ and a/w_t

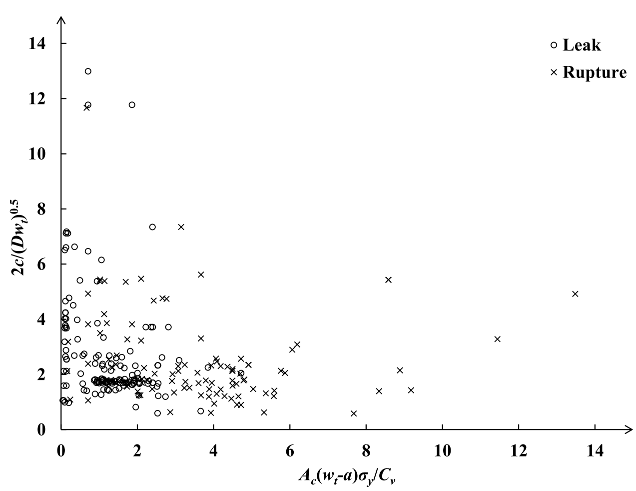

(c) Failure mode vs. $2c/(Dw_t)^{0.5}$ and $A_c(w_t\text{-}a)\sigma_y/C_v$

Fig. 4 Failure mode of all test data as a function of input features. **a** Failure mode vs. a/w_t and $2c/(Dw_t)^{0.5}$. **b** Failure mode vs. $A_c\ (w_t\text{-}a)\sigma_y/C_v$ and a/w_t. **c** Failure mode vs. $2c/(Dw_t)^{0.5}$ and $A_c\ (w_t\text{-}a)\sigma_y/C_v$

Table 3 Values of tuned hyper-parameters of five ML algorithms using ten-fold cross validation

Algorithm	Tuned hyper-parameters
NB	priors = [0.357, 0.643][a]
SVM	C = 230; γ_G = 1.3
DT	min_samples_split = 7; min_samples_leaf = 1; max_depth = 21
RF	n_estimators = 106; min_samples_split = 2; min_samples_leaf = 1; max_features = 2; max_depth = 25
GB	n_estimators = 167; min_samples_split = 7; min_samples_leaf = 4; max_depth = 5; learning_rate = 0.5

Feature importance

The feature importance quantifies the impact of a given input feature on the predictive performance of the classifier. DT and DT-based ensemble algorithms can inherently evaluate the importance of each input feature based on GI or mean squared error (MSE), which is employed as the splitting criterion for the construction of trees and forests in DT, RF and GB. The feature importance for a single DT is calculated as the total decrease of GI or MSE caused by the input feature. For DT-based ensembles, the feature importance is the average value of all trees. As such, the importance of the three input features in DT, RF and GB is quantified and shown in Table 5, where the mean and standard deviation of the importance of each feature are obtained by using 100 random states to develop each ML model. A greater mean value in the table indicates a higher importance for the corresponding feature. The random state is a parameter embedded in *scikit-learn* that guarantees the repeatability of a ML model. This is because DT and DT-based ensemble models could be developed slightly differently across different runs, even with the same hyper-parameters, as the best-found splits of decision nodes may vary across different runs. Therefore, it is valuable to investigate the feature importance of the three ML models under different random states to understand the inherent variability of these models. Results in Table 5 indicate that $A_c\ (w_t\text{-}a)\sigma_y/C_v$ is the most important input feature in the DT, RF and GB models, followed by a/w_t and then $2c/(Dw_t)^{0.5}$. Such observations are consistent with the discussions based on Fig. 4 (Section "Selection of input features"). The standard deviation of the importance of each input feature for the RF model is larger than that of the same input feature for DT and GB models, but still negligibly small compared with the mean feature importance. This observation implies that when developed at different random states, more variability exists in RF than in DT and GB models. However, such variability of feature importance can still be considered negligible.

Discussions

The results presented in the previous sections demonstrate the advantages of the ML models to predict the failure modes of pipelines containing surface cracks in comparison with the mechanics-based approach. The developed ML models can be readily employed in the fitness-for-service assessment of pipelines containing surface cracks to facilitate the decision making concerning the rehabilitation of in-service pipelines. A few limitations of the investigations should be pointed out. First, the applicability of the five ML models developed in this study is limited by the ranges of the pipe geometric and material properties of the 250 full-scale test data collected. The robustness and applicability of these ML models can be improved by expanding the full-scale test database (depending on the availability of more recent test data in the public domain), in particular those corresponding to high-strength high-toughness pipe specimens. Second, the ML models developed in this study result in a deterministic classification of the failure mode. More sophisticated models can be developed to classify the failure mode probabilistically, which will facilitate the reliability- and risk-based assessment of pipelines containing surface cracks. Finally, the ML models developed in this study are completely data driven and therefore "black-box" models. Engineers may prefer a hybrid between the mechanics-based and machine learning models (i.e. the grey-box model) for improved transparency and interpretability. This is worth exploring in the future.

Conclusions

This study applies the mechanics-based approach and five ML algorithms, including NB, SVM, DT, RF and GB, to predict the failure mode, i.e. leak or rupture, of steel oil and gas pipelines that contain longitudinally oriented surface cracks. The mechanics-based approach classifies the failure mode by comparing the nominal hoop stress remote from the surface crack at failure, σ_{hb}, and the remote nominal hoop stress to cause unstable longitudinal propagation of the through-wall crack, σ_{hr}. The CorLAS-S model is selected to compute σ_{hb}, and the Battelle and CorLAS-T models are selected to compute σ_{hr}. Among the five ML algorithms, NB, SVM and DT are single ML algorithms, and the other two are ensemble ML algorithms. Three input features, namely a/w_t, $2c/(Dw_t)^{0.5}$ and $A_c\ (w_t\text{-}a)\sigma_y/C_v$, are employed in the ML models.

A total of 250 full-scale burst tests of pipe specimens containing longitudinal surface cracks are collected from the open literature and used to evaluate the predictive performance of these ML algorithms. The analysis results indicate that while the mechanics-based approach is accurate in identifying ruptures, it misclassifies many leaks as ruptures and has an overall accuracy of about 55%. In contrast, all five

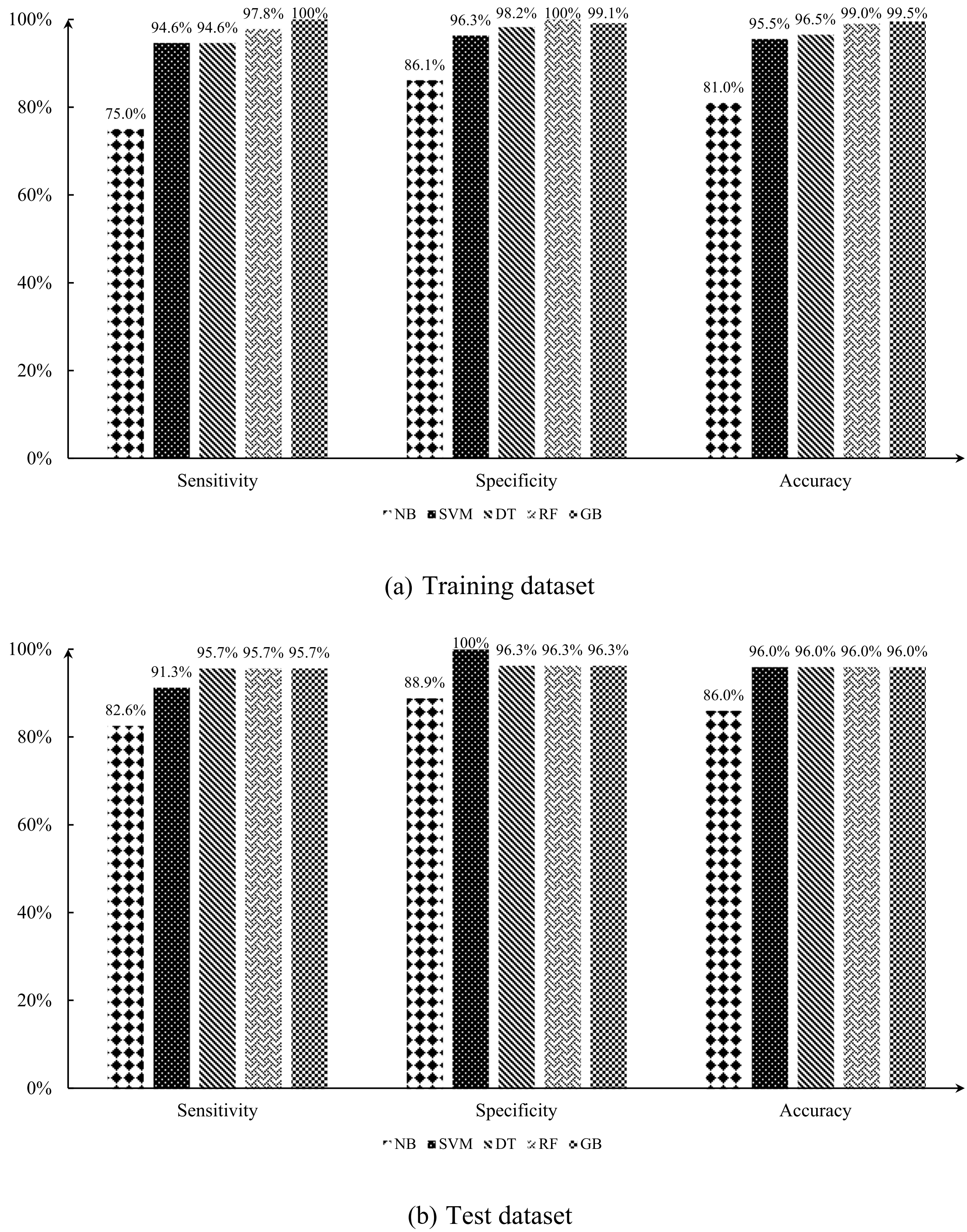

Fig. 5 Performance of five ML models on training and test datasets. **a** Training dataset. **b** Test dataset

Table 4 Confusion matrices of five ML models applied to the test dataset

(a) NB			
Total number of samples = 50		Predicted failure mode	
		Rupture (22)	Leak (28)
Actual failure mode	Rupture (23)	$n_{TP}=19$	$n_{FN}=4$
	Leak (27)	$n_{FP}=3$	$n_{TN}=24$
(b) SVM			
Total number of samples = 50		Predicted failure mode	
		Rupture (21)	Leak (29)
Actual failure mode	Rupture (23)	$n_{TP}=21$	$n_{FN}=2$
	Leak (27)	$n_{FP}=0$	$n_{TN}=27$
(c) DT			
Total number of samples = 50		Predicted failure mode	
		Rupture (23)	Leak (27)
Actual failure mode	Rupture (23)	$n_{TP}=22$	$n_{FN}=1$
	Leak (27)	$n_{FP}=1$	$n_{TN}=26$
(d) RF			
Total number of samples = 50		Predicted failure mode	
		Rupture (23)	Leak (27)
Actual failure mode	Rupture (23)	$n_{TP}=22$	$n_{FN}=1$
	Leak (27)	$n_{FP}=1$	$n_{TN}=26$
(e) GB			
Total number of samples = 50		Predicted failure mode	
		Rupture (23)	Leak (27)
Actual failure mode	Rupture (23)	$n_{TP}=22$	$n_{FN}=1$
	Leak (27)	$n_{FP}=1$	$n_{TN}=26$

Table 5 Mean and standard deviation of the feature importance of three ML models obtained by using 100 random states

Model		a/w_t	$2c/(Dw_t)^{0.5}$	$A_c\,(w_t\text{-}a)\sigma_y/C_v$
DT	Mean	0.2496	0.1238	0.6266
	Std. Dev.	0.0083	0.0059	0.0045
RF	Mean	0.3682	0.1819	0.4499
	Std. Dev.	0.0127	0.0062	0.0134
GB	Mean	0.2905	0.1539	0.5556
	Std. Dev.	0.0026	0.0026	0.0001

ML models are markedly more effective than the mechanics-based approach in identifying the failure mode. Among the five models, the predictive accuracy of the two ensemble algorithms, i.e. RF and GB, is the highest with the overall accuracy of over 95% for both the training and test datasets. The accuracy of DT and SVM is only slightly less than that of RF and GB, whereas NB has the lowest accuracy at about 80%. It is observed that $A_c\,(w_t\text{-}a)\sigma_y/C_v$ is the most important input feature, followed by a/w_t and then $2c/(Dw_t)^{0.5}$, in DT, RF and GB models. This study demonstrates the value of machine learning models for improving the pipeline integrity management practice with respect to cracks.

Appendix A

Equations for calculating J_t and J_{tT} in the CorLAS-S and CorLAS-T models

The equation for calculating J_t in the CorLAS-S model is:

$$J_t = J_e + J_p = Q_{sf} F_{sf} a\left(\frac{\pi\sigma_l^2}{E} + f_3(n)\varepsilon_p\sigma_l\right) \tag{A.1}$$

where J_e and J_p are the elastic and plastic component of J_t, respectively. The equation for calculating J_{tT} in the CorLAS-T model is:

$$J_{tT} = J_{eT} + J_{pT} = \frac{M^2\sigma_{hr}^2\pi c}{E}\sec\left(\frac{c}{3D}\right) + 2cf_3(n)M\sigma_{hr}\varepsilon_p\sqrt{\frac{3\pi D}{3\pi D - 2c}} \tag{A.2}$$

where J_{eT} and J_{pT} are the elastic and plastic component of J_{tT}, respectively. J_{eT} and J_{pT} are based on the stress intensity factor solution for through-wall cracks and Kumar et al. [41]. In Eqs. (A.1) and (A.2), Q_{sf} is the flaw shape factor given by:

$$Q_{sf} = 1.2581 - 0.20589\left(\frac{a}{2c}\right) - 11.493\left(\frac{a}{2c}\right)^2 + 29.586\left(\frac{a}{2c}\right)^3 - 23.584\left(\frac{a}{2c}\right)^4 \tag{A.3}$$

F_{sf} is the free surface factor given by:

$$F_{sf} = \begin{cases} 1.0 & \frac{a}{w_t} \le 0.01 \\ \left(\frac{2w_t}{\pi a}\right)\tan\left(\frac{\pi a}{2w_t}\right)\left(1 - \frac{2a}{2c}\right) + \frac{2a}{2c} & 0.01 < \frac{a}{w_t} \le 0.95 \\ \left[8.515 + \left(\frac{a}{w_t} - 0.95\right)\frac{4114.8}{w_t}\right]\left(1 - \frac{2a}{2c}\right) + \frac{2a}{2c} & 0.95 \le \frac{a}{w_t} \le 1.0 \end{cases} \tag{A.4}$$

$f_3(n)$ is the Shih and Hutchinson [62] factor given by:

$$f_3(n) = \left[3.85n^{-0.5}(1-n) + \pi n\right](1+n) \tag{A.5}$$

n is the strain hardening exponent [44, 46] that can be calculated by:

$$n = -0.00546 + 0.556\left(\frac{\sigma_y}{\sigma_u}\right) - 0.547\left(\frac{\sigma_y}{\sigma_u}\right)^2 \tag{A.6}$$

and ε_p is the plastic strain corresponding to σ_l for API steel given by:

$$\varepsilon_p = \left(0.005 - \frac{\sigma_y}{E}\right)\left(\frac{\sigma_l}{\sigma_y}\right)^{\frac{1}{n}} \tag{A.7}$$

Note that $2c$ in Eqs. (A.3) and (A.4) represents the (equivalent) semi-elliptical crack length.

Appendix B
Table 6

Table 6 Details of 250 full-scale burst tests of pipe specimens with surface cracks

No.	Data source	Test name	D (mm)	w_t (mm)	a (mm)	$2c$ (mm)	σ_y (MPa)	σ_u (MPa)	C_v (J)	Shape	Failure mode	Training/Test
1	Staat [63]	AA3I	88.9	4.0	0.8	79.0	336.0	486.0	76.0	SE	R	Training
2		AA3H	88.9	4.0	2.0	45.0	336.0	486.0	76.0	SE	R	Training
3		AA4A	88.9	4.0	2.0	93.0	336.0	486.0	76.0	SE	R	Test
4		AA3F	88.9	4.0	2.0	245.0	336.0	486.0	76.0	SE	L	Training
5		AA3D	88.9	4.0	2.6	102.0	336.0	486.0	76.0	SE	L	Training
6		AA3B	88.9	4.0	1.1	66.0	336.0	486.0	76.0	SE	R	Training
7		AA8A	88.9	4.0	1.0	116.0	336.0	486.0	76.0	SE	L	Training
8		AA4F	88.9	4.0	2.0	20.0	336.0	486.0	76.0	SE	R	Training
9		AA4I	88.9	4.0	2.3	27.0	336.0	486.0	76.0	SE	L	Training
10		AA3E	88.9	4.0	2.0	72.0	336.0	486.0	76.0	SE	R	Test
11		AA8E	88.9	4.0	2.0	122.0	336.0	486.0	76.0	SE	L	Training
12		AA3G	88.9	4.0	2.0	222.0	336.0	486.0	76.0	SE	L	Training
13		AA8D	88.9	4.0	2.1	220.0	336.0	486.0	76.0	SE	R	Training
14		AA3C	88.9	4.0	2.8	75.0	336.0	486.0	76.0	SE	L	Training
15		AA8C	88.9	4.0	3.0	125.0	336.0	486.0	76.0	SE	L	Training
16		AA6A	88.9	4.0	3.1	85.0	336.0	486.0	76.0	SE	L	Training
17		AA6G	88.9	4.0	3.6	40.0	336.0	486.0	76.0	SE	L	Training
18		AA6F	88.9	4.0	3.6	30.0	336.0	486.0	76.0	SE	L	Training
19		GWF01	711.2	8.2	7.8	205.0	543.0	695.0	50.0	SE	L	Test
20		GWF02	711.2	8.2	7.5	210.0	543.0	695.0	50.0	SE	L	Training
21		GWF03	711.2	8.2	7.1	200.0	543.0	695.0	50.0	SE	L	Test
22		GWF04	711.2	8.2	6.2	250.0	543.0	695.0	50.0	SE	R	Training
23		GWF05	914.4	10.6	9.2	200.0	529.0	670.0	115.0	SE	L	Test
24		GWF06	914.4	10.6	7.2	250.0	529.0	670.0	115.0	SE	R	Training
25		CA1E	88.9	4.0	2.0	72.0	512.0	642.0	44.0	SE	R	Training
26		CA1D	88.9	4.0	2.0	222.0	512.0	642.0	44.0	SE	L	Training
27		HD1A	564.0	18.4	16.8	218.0	798.0	922.0	78.0	SE	L	Training

Table 6 (continued)

No.	Data source	Test name	D (mm)	w_t (mm)	a (mm)	$2c$ (mm)	σ_y (MPa)	σ_u (MPa)	C_v (J)	Shape	Failure mode	Training/Test
28		HD2B	565.0	18.0	9.3	144.0	778.0	925.0	59.0	SE	R	Test
29		HD3	566.0	18.0	11.6	215.0	703.0	847.0	80.0	SE	R	Training
30		HD4	566.0	17.8	15.8	150.0	751.0	886.0	79.0	SE	L	Training
31		HD5	565.0	20.4	16.1	96.0	878.0	990.0	64.0	SE	R	Training
32		HD6	566.0	21.7	14.5	65.0	866.0	979.0	65.0	SE	R	Training
33		HD8	565.0	17.6	15.0	63.0	813.0	944.0	59.0	SE	R	Training
34		HD16	571.0	17.7	13.1	160.0	831.0	947.0	68.0	SE	R	Test
35		HD17	565.0	17.6	11.6	205.0	832.0	966.0	68.0	SE	R	Training
36		HD9	565.0	17.5	13.0	94.0	859.0	982.0	77.0	SE	R	Test
37		HD10	565.0	18.4	14.7	155.0	853.0	973.0	75.0	SE	R	Training
38		HD11	567.0	18.5	10.7	143.0	842.0	985.0	63.0	SE	R	Training
39		HD12	565.0	17.7	9.0	215.0	830.0	984.0	65.0	SE	R	Test
40		HD13	566.0	17.8	10.0	142.0	726.0	879.0	81.0	SE	R	Training
41		HD14	565.0	18.7	13.5	93.0	843.0	976.0	76.0	SE	R	Training
42		HD15	564.0	18.0	17.8	98.0	825.0	966.0	65.0	SE	L	Test
43		1	76.4	3.2	1.7	17.0	335.0	490.0	166.0	SE	R	Training
44		5	77.6	3.8	3.2	17.0	335.0	490.0	166.0	SE	L	Training
45		6	76.4	3.2	2.4	45.0	335.0	490.0	166.0	SE	L	Test
46		7	76.8	3.4	2.8	65.0	335.0	490.0	166.0	SE	L	Training
47		8	76.8	3.4	2.6	115.0	335.0	490.0	166.0	SE	L	Training
48		9	76.8	3.4	2.3	115.0	335.0	490.0	166.0	SE	L	Training
49		10	76.8	3.4	2.6	65.0	335.0	490.0	166.0	SE	L	Training
50		11	77.6	3.8	3.1	65.0	335.0	490.0	166.0	SE	L	Test
51		19	77.6	3.8	3.0	80.0	305.0	454.0	168.0	SE	L	Training
52		F5	88.9	4.0	3.7	20.0	246.0	570.0	84.0	SE	L	Training
53		F6	88.9	4.0	3.8	20.0	246.0	570.0	84.0	SE	L	Test
54		F7	88.9	4.0	3.7	30.0	246.0	570.0	84.0	SE	L	Test

Table 6 (continued)

No.	Data source	Test name	D (mm)	w_t (mm)	a (mm)	$2c$ (mm)	σ_y (MPa)	σ_u (MPa)	C_v (J)	Shape	Failure mode	Training/Test
55		F8	88.9	4.0	3.3	40.0	246.0	570.0	84.0	SE	R	Training
56		F9	88.9	4.0	3.7	40.0	246.0	570.0	84.0	SE	L	Training
57		F10	88.9	4.0	3.5	50.0	246.0	570.0	84.0	SE	L	Training
58		F11	88.9	4.0	3.2	60.0	246.0	570.0	84.0	SE	R	Training
59		F12	88.9	4.0	3.6	60.0	246.0	570.0	84.0	SE	L	Training
60		F13	88.9	4.0	3.5	80.0	246.0	570.0	84.0	SE	L	Training
61		F14	88.9	4.0	3.5	80.0	246.0	570.0	84.0	SE	L	Training
62		F15	88.9	4.0	3.1	90.0	246.0	570.0	84.0	SE	L	Training
63		846,077	1422.4	19.3	10.4	180.0	740.0	774.0	261.0	REC	R	Training
64		846,014	1422.4	20.1	3.8	385.0	795.0	840.0	171.0	REC	R	Training
65		99,457	914.4	16.4	9.0	150.0	739.0	813.0	253.0	REC	R	Training
66		99,457	914.4	16.4	6.0	450.0	739.0	813.0	253.0	REC	R	Training
67	Hosseini et al. [31]	CR1	508.0	5.7	2.2	200.0	433.0	618.0	43.5	SE	L	Training
68		CR2	508.0	5.7	2.7	200.0	433.0	618.0	43.5	SE	L	Test
69		CR3	508.0	5.7	2.7	200.0	433.0	618.0	43.5	SE	L	Training
70		CR4	508.0	5.7	2.9	200.0	433.0	618.0	43.5	SE	L	Training
71	Cravero and Ruggieri [20]	3*60	508.0	15.8	3.0	60.0	483.0	597.0	135.0	SE	L	Training
72		7*140	508.0	15.8	7.0	140.0	483.0	597.0	135.0	SE	L	Training
73		10*200	508.0	15.8	10.0	200.0	483.0	597.0	135.0	SE	L	Training
74	Kiefner et al. [40]	18--10	762.0	9.8	6.0	219.2	420.6	563.3	61.0	REC	R	Training
75		18--11	762.0	9.7	5.9	369.8	420.6	563.3	61.0	REC	R	Training
76		18--13	762.0	10.0	9.2	224.0	420.6	563.3	61.0	REC	L	Training
77		18--15	762.0	9.6	7.7	224.0	417.8	560.5	54.9	REC	L	Training
78		18--31	762.0	9.7	5.8	83.8	394.4	530.9	59.0	REC	L	Training
79		18--32	762.0	9.7	5.8	83.8	394.4	530.9	59.0	REC	R	Training
80		18--38	762.0	9.3	3.6	370.8	440.6	575.0	54.9	REC	R	Training
81		18--39	762.0	9.6	3.9	222.3	440.6	575.0	54.9	REC	R	Training
82		18--40	762.0	9.6	3.9	83.8	440.6	575.0	54.9	REC	R	Training
83		18--41	762.0	9.9	8.1	370.8	439.9	553.6	61.0	REC	R	Training
84		18--42	762.0	9.9	8.1	86.4	439.9	553.6	61.0	REC	L	Training
85		18--61	914.4	10.0	5.1	84.6	509.5	632.9	44.7	REC	R	Training

Table 6 (continued)

No.	Data source	Test name	D (mm)	w_t (mm)	a (mm)	$2c$ (mm)	σ_y (MPa)	σ_u (MPa)	C_v (J)	Shape	Failure mode	Training/Test
86		18--66	914.4	10.1	5.1	153.2	504.0	633.6	42.7	REC	R	Training
87		18--70	914.4	11.2	6.8	139.7	379.2	536.4	56.9	REC	L	Training
88		18--73	914.4	11.3	8.7	139.7	379.2	536.4	56.9	REC	L	Training
89		18--74	914.4	9.7	5.0	190.5	475.7	618.5	44.7	REC	R	Training
90		18--89	762.0	9.1	4.7	152.4	448.2	583.3	40.7	REC	R	Training
91		18--90	762.0	9.3	4.6	152.4	448.2	583.3	40.7	REC	R	Training
92		18--91	762.0	9.5	4.5	152.4	448.2	583.3	40.7	REC	R	Test
93		69--5	914.4	9.7	5.1	228.6	474.4	604.0	28.5	REC	R	Training
94		69--11	914.4	10.0	7.6	213.4	449.5	609.5	46.8	REC	L	Training
95		69--11	914.4	10.0	7.5	121.9	449.5	609.5	46.8	REC	L	Test
96		69--18	762.0	15.5	10.9	406.4	456.4	627.4	63.0	REC	R	Training
97		69--22	762.0	15.6	10.9	406.4	456.4	627.4	63.0	REC	R	Training
98		70--6	863.6	12.8	3.2	406.4	465.4	613.6	26.4	REC	R	Training
99		70--9	863.6	12.9	11.2	609.6	465.4	613.6	26.4	REC	L	Training
100		70--9	863.6	12.9	10.7	609.6	465.4	613.6	26.4	REC	R	Training
101		70--18	914.4	10.6	4.3	165.1	456.4	609.5	50.8	REC	R	Test
102		70--21	914.4	10.3	5.2	111.8	449.5	609.5	46.8	REC	R	Training
103		70--24	1066.8	10.3	6.5	165.1	435.1	586.1	44.7	REC	R	Training
104		70--27	914.4	9.8	6.9	152.4	484.7	610.2	24.4	REC	L	Training
105		71--6	914.4	10.7	7.5	63.5	423.3	587.4	54.9	REC	L	Training
106		71--7	914.4	11.1	7.6	127.0	397.8	562.6	69.1	REC	L	Training
107		71--23	1066.8	12.0	6.0	292.1	479.2	NG	20.3	REC	R	Training
108		71--24	914.4	9.9	5.0	406.4	484.7	NG	22.4	REC	R	Training
109		71--25	914.4	9.9	5.0	406.4	484.7	NG	22.4	REC	R	Training
110	Rana and Rawls [57]	71,116	236.7	7.4	4.6	50.8	1096.3	1179.0	43.1	SE	R	Test
111		71,117	236.7	7.5	5.2	50.8	1096.3	1179.0	43.1	SE	R	Training
112		71,103	237.0	7.6	5.7	50.8	1096.3	1179.0	43.1	SE	R	Training
113		71,137	236.2	7.5	5.2	69.9	1096.3	1179.0	43.1	SE	R	Training
114		91,103	236.5	7.4	5.6	50.8	1054.9	1137.6	34.5	SE	R	Training
115		91,107	236.7	7.2	5.8	69.9	1054.9	1137.6	34.5	SE	R	Training
116	Staat [63]	13	78.0	4.0	3.1	45.0	335.0	490.0	166.0	SE	L	Training
117		14	77.8	3.9	3.1	65.0	335.0	490.0	166.0	SE	L	Training
118		15	77.8	3.9	3.1	115.0	335.0	490.0	166.0	SE	L	Training
119		16	78.0	4.0	3.1	45.0	335.0	490.0	166.0	SE	L	Training

Table 6 (continued)

No.	Data source	Test name	D (mm)	w_t (mm)	a (mm)	$2c$ (mm)	σ_y (MPa)	σ_u (MPa)	C_v (J)	Shape	Failure mode	Training/Test
120		17	78.0	4.0	3.4	65.0	335.0	490.0	166.0	SE	L	Training
121		18	78.0	4.0	3.4	115.0	335.0	490.0	166.0	SE	L	Training
122		12	78.0	4.0	3.1	65.0	335.0	490.0	166.0	SE	L	Training
123		20	77.8	3.9	2.9	125.0	305.0	454.0	168.0	SE	L	Training
124	Rana and Selines [58]	71,106	237.0	7.0	4.3	25.4	1096.3	1179.0	43.1	SE	R	Training
125		71,126	236.5	7.4	5.4	25.4	1096.3	1179.0	43.1	SE	R	Training
126		71,125	236.7	7.8	6.5	25.4	1096.3	1179.0	43.1	SE	L	Training
127		71,118	237.2	7.6	6.2	50.8	1096.3	1179.0	43.1	SE	L	Training
128		71,138	236.7	7.4	6.3	69.9	1096.3	1179.0	43.1	SE	L	Training
129		71,139	236.5	7.4	7.2	69.9	1096.3	1179.0	43.1	SE	L	Training
130		71,132	237.2	7.1	6.1	69.9	1096.3	1179.0	43.1	SE	L	Training
131		71,133	236.5	7.4	6.7	69.9	1096.3	1179.0	43.1	SE	L	Test
132		71,119	236.5	7.4	5.1	76.2	1096.3	1179.0	43.1	SE	R	Training
133		71,120	237.0	7.7	5.5	76.2	1096.3	1179.0	43.1	SE	R	Training
134		71,124	236.5	7.1	6.1	76.2	1096.3	1179.0	43.1	SE	L	Training
135		91,105	236.5	7.3	6.2	50.8	1054.9	1137.6	34.5	SE	L	Training
136		91,109	236.7	7.3	6.3	69.9	1054.9	1137.6	34.5	SE	L	Test
137	Rana et al. [59]	B13	230.0	7.3	5.8	94.9	683.0	847.0	51.2	SE	L	Test
138		B14	230.0	6.8	4.8	88.4	683.0	847.0	51.2	SE	R	Training
139		B15	230.0	7.2	4.3	93.6	683.0	847.0	51.2	SE	R	Training
140		B16	230.0	7.3	5.5	94.9	683.0	847.0	51.2	SE	L	Training
141		B17	230.0	6.9	4.9	89.7	890.0	949.0	105.6	SE	R	Test
142		B18	230.0	7.6	5.5	98.8	890.0	949.0	105.6	SE	R	Training
143		B19	230.0	7.8	5.9	101.4	890.0	949.0	105.6	SE	L	Training
144		B20	230.0	7.3	5.7	94.9	890.0	949.0	105.6	SE	L	Training
145		B21	230.0	7.7	6.1	100.1	890.0	949.0	105.6	SE	L	Training
146		B22	230.0	7.8	6.5	101.4	890.0	949.0	105.6	SE	L	Training
147		B23	230.0	6.8	5.1	68.0	655.0	778.0	49.6	SE	R	Training
148		B24	230.0	6.6	5.3	66.0	657.0	788.0	40.8	SE	L	Training
149		B25	230.0	6.9	5.9	103.5	755.0	870.0	43.2	SE	L	Test
150		B29	236.0	9.2	7.4	92.0	648.0	786.0	51.2	SE	L	Training
151		B30	236.0	9.7	7.3	97.0	648.0	786.0	51.2	SE	R	Training
152		B31	236.0	9.9	7.9	99.0	648.0	786.0	51.2	SE	L	Training
153		B35	178.0	5.4	2.7	40.7	570.0	776.0	22.4	SE	R	Test

Table 6 (continued)

No.	Data source	Test name	D (mm)	w_t (mm)	a (mm)	$2c$ (mm)	σ_y (MPa)	σ_u (MPa)	C_v (J)	Shape	Failure mode	Training/Test
154		B36	178.0	5.5	3.2	40.6	577.0	774.0	25.6	SE	R	Test
155		B37	178.0	5.6	4.0	42.4	584.0	817.0	25.6	SE	R	Training
156		B38	178.0	5.1	4.0	37.6	625.0	783.0	25.6	SE	R	Training
157		B39	178.0	5.2	4.7	39.1	623.0	797.0	25.6	SE	L	Training
158		B40	178.0	5.1	2.6	44.4	587.0	762.0	23.2	SE	R	Training
159		B41	178.0	5.4	3.2	44.9	563.0	808.0	23.2	SE	R	Training
160		B42	178.0	5.5	3.9	47.4	577.0	800.0	23.2	SE	R	Training
161		B43	178.0	5.3	4.2	45.3	635.0	811.0	23.2	SE	R	Training
162		B44	178.0	5.2	4.7	44.2	604.0	825.0	23.2	SE	L	Training
163		B45	178.0	5.5	2.8	55.9	541.0	826.0	24.8	SE	R	Training
164		B46	178.0	5.4	3.1	52.7	536.0	736.0	24.8	SE	R	Training
165		B47	178.0	5.3	3.8	54.4	582.0	802.0	24.8	SE	R	Training
166		B48	178.0	5.3	4.2	52.2	560.0	811.0	24.8	SE	R	Training
167		B49	178.0	5.3	4.8	53.3	630.0	832.0	24.8	SE	L	Test
168		B50	178.0	5.3	2.6	65.1	670.0	815.0	24.8	SE	R	Test
169		B51	178.0	5.0	3.1	65.8	599.0	808.0	20.0	SE	R	Training
170		B52	178.0	4.9	3.4	61.1	595.0	796.0	20.0	SE	R	Training
171		B53	178.0	5.4	4.2	66.0	643.0	829.0	20.0	SE	R	Training
172		B54	178.0	5.4	4.9	67.5	557.0	838.0	20.0	SE	L	Training
173		B55	178.0	5.4	4.3	81.2	615.0	823.0	20.0	SE	L	Test
174		B56	178.0	5.0	3.0	76.2	619.0	831.0	20.0	SE	R	Test
175		B57	178.0	5.1	3.5	74.5	603.0	787.0	19.2	SE	R	Training
176		B58	178.0	5.2	4.1	76.4	665.0	843.0	19.2	SE	L	Test
177		B59	178.0	5.5	4.9	82.4	623.0	811.0	19.2	SE	L	Training
178		B60	232.0	6.6	5.5	65.1	748.0	875.0	32.0	SE	L	Training
179		B61	232.0	6.2	5.2	62.0	713.0	824.0	31.2	SE	L	Training
180		B62	232.0	6.4	5.5	65.9	763.0	872.0	51.2	SE	L	Training
181		C1	229.0	6.8	4.8	68.0	878.0	996.0	100.0	SE	R	Training
182		C2	229.0	6.8	4.8	68.0	878.0	996.0	100.0	SE	R	Training
183		C3	229.0	6.7	4.7	67.0	878.0	996.0	100.0	SE	R	Training
184		C4	229.0	6.8	5.1	68.0	878.0	996.0	100.0	SE	L	Training
185		C5	229.0	6.7	5.0	67.0	878.0	996.0	100.0	SE	L	Training
186		C6	229.0	6.8	4.9	68.0	878.0	996.0	100.0	SE	R	Training
187		C7	229.0	6.8	4.4	68.0	878.0	996.0	100.0	SE	R	Test

Table 6 (continued)

No.	Data source	Test name	D (mm)	w_t (mm)	a (mm)	$2c$ (mm)	σ_y (MPa)	σ_u (MPa)	C_v (J)	Shape	Failure mode	Training/Test
188		C8	229.0	6.8	4.8	68.0	878.0	996.0	100.0	SE	R	Training
189		C9	229.0	6.8	5.1	68.0	887.0	989.0	100.0	SE	L	Test
190		C10	229.0	6.7	5.0	67.0	867.0	982.0	100.0	SE	L	Training
191		C11	229.0	6.9	5.5	69.0	855.0	961.0	100.0	SE	L	Test
192		C12	229.0	6.6	5.3	66.0	878.0	996.0	100.0	SE	L	Training
193		C13	229.0	6.5	5.1	65.0	878.0	996.0	100.0	SE	L	Training
194		C14	203.0	6.7	5.0	67.0	852.0	964.0	102.4	SE	L	Training
195		C15	203.0	6.7	5.0	67.0	852.0	964.0	102.4	SE	L	Training
196		C16	203.0	6.6	5.0	66.0	852.0	964.0	102.4	SE	L	Test
197		C17	203.0	6.7	5.4	67.0	852.0	964.0	102.4	SE	L	Training
198		C18	203.0	6.5	5.2	65.0	852.0	964.0	102.4	SE	L	Training
199		C19	203.0	6.5	5.1	65.0	852.0	964.0	102.4	SE	L	Training
200		C20	203.0	6.6	4.6	66.0	852.0	964.0	102.4	SE	R	Training
201		C21	203.0	6.7	4.4	67.0	852.0	964.0	102.4	SE	R	Training
202		C22	203.0	6.4	4.8	64.0	852.0	964.0	102.4	SE	L	Test
203		C23	203.0	6.5	4.9	65.0	852.0	964.0	102.4	SE	L	Test
204		C24	203.0	6.4	4.5	64.0	852.0	964.0	102.4	SE	R	Test
205		C25	203.0	6.2	4.3	62.0	852.0	964.0	102.4	SE	R	Test
206		C26	203.0	6.4	4.6	64.0	852.0	964.0	102.4	SE	R	Test
207		C27	230.0	7.5	5.5	97.5	898.0	1000.0	29.6	SE	R	Test
208		C28	230.0	7.5	5.5	97.5	898.0	1000.0	29.6	SE	R	Training
209		C29	230.0	6.9	5.3	89.7	898.0	1000.0	29.6	SE	L	Training
210		C30	230.0	7.1	5.7	71.0	898.0	1000.0	52.8	SE	L	Training
211		C31	230.0	6.5	5.1	65.0	898.0	1000.0	52.8	SE	L	Training
212		C32	230.0	7.4	5.7	96.2	850.0	950.0	45.6	SE	L	Training
213		C33	230.0	7.4	5.7	96.2	850.0	950.0	45.6	SE	L	Training
214		C34	230.0	7.5	5.3	97.5	850.0	950.0	45.6	SE	R	Training
215		C35	230.0	7.3	5.7	73.0	922.0	1000.0	31.2	SE	R	Training
216		C36	230.0	6.9	5.5	69.0	922.0	1000.0	31.2	SE	R	Test
217		C38	230.0	6.6	5.0	66.0	835.0	966.0	65.6	SE	L	Training
218		C39	230.0	7.0	5.6	70.0	835.0	966.0	65.6	SE	L	Test
219		C40	230.0	6.8	5.1	68.0	835.0	966.0	65.6	SE	R	Training
220		C41	230.0	7.4	5.2	74.0	835.0	966.0	65.6	SE	R	Test
221		C42	230.0	7.4	5.2	74.0	835.0	966.0	65.6	SE	R	Training

Table 6 (continued)

No.	Data source	Test name	D (mm)	w_t (mm)	a (mm)	$2c$ (mm)	σ_y (MPa)	σ_u (MPa)	C_v (J)	Shape	Failure mode	Training/Test
222		C43	230.0	7.5	5.6	75.0	835.0	966.0	65.6	SE	L	Test
223		C44	230.0	7.5	5.6	75.0	835.0	966.0	65.6	SE	L	Training
224		C45	203.0	6.8	5.0	68.0	850.0	960.0	72.0	SE	L	Test
225		C46	203.0	6.9	4.8	69.0	850.0	960.0	72.0	SE	R	Test
226		C47	203.0	6.5	4.6	65.0	850.0	960.0	72.0	SE	L	Training
227		C48	203.0	6.6	5.0	66.0	850.0	960.0	72.0	SE	L	Training
228		C49	203.0	6.8	4.6	68.0	850.0	960.0	72.0	SE	R	Test
229		C50–1	203.0	6.8	4.6	68.0	850.0	960.0	72.0	SE	R	Training
230		C50–2	235.0	6.8	5.8	68.0	896.0	1000.0	30.4	SE	L	Training
231		C51	235.0	6.8	5.8	68.0	896.0	1000.0	30.4	SE	L	Training
232		C56	235.0	6.6	5.6	66.0	793.0	862.0	50.4	SE	L	Training
233		C67	191.0	6.5	5.5	65.0	842.0	962.0	61.6	SE	L	Training
234		C68	191.0	6.5	5.5	65.0	842.0	962.0	61.6	SE	L	Training
235		C69	191.0	6.3	5.4	63.0	969.0	1067.0	44.8	SE	L	Training
236		C70	232.0	4.7	4.1	46.6	999.0	1072.0	78.4	SE	L	Training
237		C71	232.0	4.8	3.9	47.5	921.0	985.0	41.6	SE	L	Test
238		C72	232.0	4.9	4.2	49.0	921.0	985.0	41.6	SE	L	Training
239		C73	232.0	4.7	4.0	47.0	921.0	985.0	41.6	SE	L	Training
240		C74	232.0	4.7	4.0	47.0	921.0	985.0	41.6	SE	L	Test
241	Kawaguchi et al. [37]	Case 1	762.0	17.5	13.6	350.0	673.0	723.0	175.0	REC	R	Training
242		Case 2	762.0	17.5	14.4	350.0	673.0	723.0	175.0	REC	L	Training
243	Amano and Makino [2]	W2	914.4	19.4	12.6	560.0	779.0	843.0	249.0	REC	R	Training
244		W3	914.4	19.2	14.6	560.0	775.0	847.0	251.0	REC	R	Training
245		W4	914.4	19.2	15.2	560.0	775.0	840.0	247.0	REC	R	Training
246		W5	914.4	19.2	15.4	560.0	775.0	840.0	247.0	REC	L	Training
247		W6	914.4	19.2	13.3	280.0	771.0	834.0	249.0	REC	R	Training
248		W7	914.4	19.3	14.2	280.0	770.0	841.0	249.0	REC	L	Training
249		W8	914.4	19.2	15.3	280.0	779.0	846.0	249.0	REC	L	Training
250		W9	914.4	19.3	17.0	280.0	770.0	841.0	249.0	REC	L	Training

1. In the Shape column, SE and REC denote semi-elliptical and rectangular crack profile, respectively
2. In the Failure mode column, R and L denote rupture and leak, respectively
3. No. 116–123 are obtained from the same reference as No. 1–66; they are separately listed since these pipe specimens have D/w_t that equal to 19.50 and 19.95
4. No. 1–5 are specimens with internal cracks; Crack positions of No. 25, 26, 43–51 and 116–123 are not reported in [63], and the other specimens have external cracks
5. The CorLAS-S model is not applicable to No. 107–115 and 124–136, as described in Section "Full-scale burst tests of pipes containing longitudinal surface cracks"
6. No. 107–109 do not provide σ_u so that they are marked as NG (not given) in the table

Appendix C

Table 7

Table 7 Search spaces of hyper-parameters during their tuning processes

Algorithm	Hyper-parameter	Search space
NB	prior of leak	[0.001, 0.999]
SVM	*C*	[50, 500]
	γ_G	[0.5, 2]
DT	min_samples_split	[2, 10]
	min_samples_leaf	[1, 5]
	max_depth	[1, 50]
RF	n_estimators	[10, 200]
	min_samples_split	[2, 10]
	min_samples_leaf	[1, 5]
	max_features	[1, 3]
	max_depth	[1, 50]
GB	n_estimators	[10, 300]
	min_samples_split	[2, 10]
	min_samples_leaf	[1, 5]
	max_depth	[1, 50]
	learning_rate	[0.01, 1]

Acknowledgements
The financial support provided by the Natural Sciences and Engineering Research Council of Canada (NSERC) through the Discovery Grant (Grant No. RGPIN-2019-05160) is gratefully acknowledged. The financial support provided to HS by the Faculty of Engineering at the University of Western Ontario is also acknowledged. The constructive comments from the anonymous reviewers are greatly appreciated.

Authors' contributions
Sun, H.: Conceptualization, Methodology, Data Acquisition, Investigation, Writing – Original Draft, Visualization. Zhou, W.: Conceptualization, Methodology, Writing – Reviewing and Editing, Supervision, Funding Acquisition. The author(s) read and approved the final manuscript.

Funding
Natural Sciences and Engineering Research Council of Canada (NSERC) Discovery Grant (Grant No. RGPIN-2019-05160) for WZ.

Availability of data and materials
The dataset of 250 full-scale burst tests of pipe specimens employed in the present study is already included in Appendix B of the manuscript. The source code of the machine learning models developed in the present study will be provided by the corresponding author upon request.

Declarations

Ethics approval and consent to participate
Not applicable.

Competing interests
The authors declare that they have no known competing financial interests or personal relationships that could have appeared to influence the work reported in this paper.

Received: 21 September 2022 Revised: 1 November 2022 Accepted: 3 November 2022
Published online: 20 January 2023

References
1. Alpaydin E (2020) Introduction to machine learning, 4th edn. The MIT Press, Cambridge
2. Amano T, Makino H (2012) Evaluation of leak/rupture behavior for axially part-through-wall notched high-strength line pipes. Proceedings of International Pipeline Conference 2012, IPC 2012-90216, Calgary. https://doi.org/10.1115/IPC2012-90216
3. American Petroleum Institute (2016) API 579–1/ASME FFS-1-fitness for service. API Recommended Practice, New York
4. Anderson T (2015) Development of a modern assessment method for longitudinal seam weld cracks. PRCI catalogue no. PR-460-134506-R0. Pipeline Research Council International, Chantilly
5. Anderson T (2017) Assessing crack-like flaws in longitudinal seam welds: a state-of-the-art review. PRCI catalogue no. PR-460-134506-R02. Pipeline Research Council International, Chantilly
6. Bergstra J, Bengio Y (2012) Random search for hyper-parameter optimization. J Mach Learn Res 13(2):281–305 https://dl.acm.org/doi/10.5555/2188385.2188395
7. Bramer M (2013) Principles of data mining, 2nd edn. Springer. https://doi.org/10.1007/978-1-4471-4884-5
8. Breiman L (2001) Random forests. Mach Learn 45(1):5–32. https://doi.org/10.1023/A:1010933404324
9. Breiman L, Friedman JH, Olshen RA, Stone CJ (1984) Classification and regression trees. Chapman & Hall/CRC
10. British Standards Institution (2019) BS7910: Guide to methods for assessing the acceptability of flaws in metallic structures, British Standards Institution, London, UK
11. Bubbico R (2018) A statistical analysis of causes and consequences of the release of hazardous materials from pipelines. The influence of layout. J Loss Prev Process Ind 56:458–466. https://doi.org/10.1016/j.jlp.2018.10.006
12. Burges CJ (1998) A tutorial on support vector machines for pattern recognition. Data Min Knowl Disc 2(2):121–167. https://doi.org/10.1023/A:1009715923555
13. Carvalho AA, Rebello JMA, Sagrilo LVS, Camerini CS, Miranda IVJ (2006) MFL signals and artificial neural networks applied to detection and classification of pipe weld defects. NDT E Int 39(8):661–667. https://doi.org/10.1016/j.ndteint.2006.04.003
14. CEPA (2015) Committed to safety, committed to Canadians: 2015 pipeline industry performance report. Canadian Energy Pipeline Association, Calgary
15. CEPA (2021) Canadian energy evolving for tomorrow: transmission pipeline industry performance report. Canadian Energy Pipeline Association, Calgary
16. Cheng YF (2013) Stress corrosion cracking of pipelines, 1st edn. John Wiley & Sons, Inc, Hoboken
17. Chicco D, Jurman G (2020) The advantages of the Matthews correlation coefficient (MCC) over F1 score and accuracy in binary classification evaluation. BMC Genomics 21(1):1–13. https://doi.org/10.1186/s12864-019-6413-7
18. Cortes C, Vapnik V (1995) Support-vector networks. Mach Learn 20(3):273–297. https://doi.org/10.1007/BF00994018
19. Cosham A, Hopkins P, Leis B (2012) Crack-like defects in pipelines: the relevance of pipeline-specific methods and standards. Proceedings of International Pipeline Conference 2012, IPC 2012-90459, Calgary. https://doi.org/10.1115/IPC2012-90459
20. Cravero S, Ruggieri C (2006) Structural integrity analysis of axially cracked pipelines using conventional and constraint-modified failure assessment diagrams. Int J Pressure Vessel Piping 83(8):607–617. https://doi.org/10.1016/j.ijpvp.2006.04.004
21. Cruz FC, Simas Filho EF, Albuquerque MCS, Silva IC, Farias CTT, Gouvea LL (2017) Efficient feature selection for neural network based detection of flaws in steel welded joints using ultrasound testing. Ultrasonics 73:1–8. https://doi.org/10.1016/j.ultras.2016.08.017
22. DNV GL, 2022. CorLAS™. https://store.veracity.com/corlas (Accessed 25 April 2022)
23. Dugdale DS (1960) Yielding of steel sheets containing slits. J Mech Phys Solids 8(2):100–104. https://doi.org/10.1016/0022-5096(60)90013-2
24. EDF Energy (2013) R6: assessment of the integrity of the structures containing defects, amendment 10 R6, revision 4, Gloucester, UK

25. Feng D, Liu Z, Wang X, Jiang Z, Liang S (2020) Failure mode classification and bearing capacity prediction for reinforced concrete columns based on ensemble machine learning algorithm. Adv Eng Inform 45:101126. https://doi.org/10.1016/j.aei.2020.101126
26. Folias ES (1964) The stresses in a cylindrical shell containing an axial crack. Int J Fract Mech 1(2):104–113. https://doi.org/10.1007/BF00186748
27. Friedman JH (2001) Greedy function approximation: a gradient boosting machine. Ann Stat 29(5):1189–1232. https://doi.org/10.1214/aos/1013203451
28. Guo L, Niffenegger M, Jing Z (2021) Statistical inference and performance evaluation for failure assessment models of pipeline with external axial surface cracks. Int J Press Vessel Pip 194 A:104480. https://doi.org/10.1016/j.ijpvp.2021.104480
29. Hastie T, Tibshirani R, Friedman JH (2009) The elements of statistical learning: data mining, inference, and prediction, 2nd edn. Springer, New York. https://doi.org/10.1007/978-0-387-84858-7
30. He Z, Zhou W (2022) Improvement of burst capacity model for pipelines containing dent-gouges using Gaussian process regression. Eng Struct 272:115028. https://doi.org/10.1016/j.engstruct.2022.115028
31. Hosseini A, Cronin D, Plumtree A, Kania R (2010) Experimental testing and evaluation of crack defects in line pipe. Proceedings of International Pipeline Conference 2010, IPC 2010-31158, Calgary. https://doi.org/10.1115/IPC2010-31158
32. James G, Witten D, Hastie T, Tibshirani R (2013) An introduction to statistical learning: with applications in R, 1st edn. Springer, New York. https://doi.org/10.1007/978-1-4614-7138-7
33. Jaske CE, Beavers JA (1996) Effect of corrosion and stress-corrosion cracking on pipe integrity and remaining life. Proceedings of the second international symposium on the mechanical integrity of process piping, St. Louis, MTI Publication No 48, pp 287–297
34. Jaske CE, Beavers JA (2001) Integrity and remaining life of pipe with stress corrosion cracking. PRCI 186-9709, catalogue no. L51928, Pipeline Research Council International, Falls Church
35. Jaske CE, Beavers JA (2002) Development and evaluation of improved model for engineering critical assessment of pipelines. Proceedings of International Pipeline Conference 2002, IPC 2002-27027, Calgary. https://doi.org/10.1115/IPC2002-27027
36. Kawaguchi S, Hagiwara N, Masuda T, Toyoda M (2004) Evaluation of leak-before-break (LBB) behavior for axially notched X65 and X80 line pipes. J Offshore Mech Arctic Eng 126(4):350–357. https://doi.org/10.1115/1.1834619
37. Kawaguchi S, Hagiwara N, Ohata M, Toyoda M (2004) Modified equation to predict leak/rupture criteria for axially through-wall notched X80 and X100 linepipes having higher Charpy energy. Proceedings of International Pipeline Conference 2004, IPC 2004-322, Calgary. https://doi.org/10.1115/IPC2004-0322
38. Kiefner JF (2008) Modified equation aids integrity management. Oil Gas J 106(37):78–82
39. Kiefner JF (2008) Modified ln-secant equation improves failure prediction. Oil Gas J 106(38):64–66
40. Kiefner JF, Maxey WA, Eiber RJ, Duffy AR (1973) Failure stress levels of flaws in pressurized pipelines, vol ASTM-STP536, pp 461–481. https://doi.org/10.1520/STP49657S
41. Kumar V, German MD, Shih CF (1981) An engineering approach for elastic-plastic fracture analysis. EPRI Report NP-1931,. Electric Power Research Institute, Palo Alto. https://doi.org/10.2172/6068291
42. Lam C, Zhou W (2015) Development of probability of ignition model for ruptures of onshore natural gas transmission pipelines. J Pressure Vessel Technol Trans ASME 138(4):041701. https://doi.org/10.1115/1.4031812
43. Lam, C., Zhou, W., 2016. Statistical analyses of incidents on onshore gas transmission pipelines based on PHMSA database. Int J Press Vessel Pip 145: 29–40. hhttps://doi.org/10.1016/j.ijpvp.2016.06.003
44. Leis BN (1992) Ductile fracture and mechanical behavior of typical X42 and X80 line-pipe steels. NG-18 Report No. 204, Pipeline Research Committee of the American Gas Association, Inc, Washington, D.C.
45. Leis BN, Ghadiali ND (1994) Pipe axial flaw failure criteria PAFFC version 1.0 user's manual and software. PRCI catalogue no. L51720. Pipeline research council international, Chantilly
46. Leis BN, Walsh WJ, Brust FW (1990) Mechanical behavior of selected line-pipe steels. NG-18 Report No. 192,. Pipeline Research Committee of the American Gas Association, Inc., Washington, D.C.
47. Liu B, Hou D, Huang P, Liu B, Tang H, Zhang W, Chen P, Zhang G (2013) An improved PSO-SVM model for online recognition defects in eddy current testing. Nondestruct Test Eval 28(4):367–385. https://doi.org/10.1080/10589759.2013.823608
48. Maimon OZ, Rokach L (2014) Data mining with decision. Theory and Applications, second ed. World Scientific, Trees. https://doi.org/10.1142/9097
49. Marani A, Nehdi ML (2020) Machine learning prediction of compressive strength for phase change materials integrated cementitious composites. Constr Build Mater 265:120286. https://doi.org/10.1016/j.conbuildmat.2020.120286
50. Maxey WA, Kiefner JF, Eiber RJ, Duffey AR (1972) Ductile fracture initiation, propagation, and arrest in cylindrical vessels. Fracture Toughness. Proceedings of the 1971 National Symposium on Fracture Mechanics, Part II, ASTM STP 514, American Society for Testing and Materials, pp 70–81
51. Moraes RM, Machado LS (2009) Gaussian naïve bayes for online training assessment in virtual reality-based simulators. Mathware Soft Comput 16(2):123–132
52. Nessim WA, Zhou W, Zhou J, Rothwell B (2009) Target reliability levels for design and assessment of onshore natural gas pipelines. J Pressure Vessel Technol Transact ASME 131(6):061701. https://doi.org/10.1115/1.3110017
53. Pedregosa F, Varoquaux G, Michel V, Thirion B, Grisel O, Blondel M, Prettenhofer P, Weiss R, Dubourg V, Vanderplas J, Passos A, Cournapeau D, Brucher M, Perrot M, Duchesnay E (2011) Scikit-learn: machine learning in Python. J Mach Learn Res 12:2825–2830
54. PHMSA, 2019. Pipeline safety: safety of gas transmission pipelines. Docket no. PHMSA-2011-0023
55. Polasik S, Jaske CE, Bubenik TA (2016) Review of engineering fracture mechanics model for pipeline applications. Proceedings of 2016 international pipeline conference. IPC 2016-64605, Calgary. https://doi.org/10.1115/IPC2016-64605
56. Rachman A, Zhang T, Ratnayake RC (2021) Applications of machine learning in pipeline integrity management: a state-of-the-art review. Int J Press Vessel Pip 193:104471. https://doi.org/10.1016/j.ijpvp.2021.104471
57. Rana MD, Rawls GB (2007) Prediction of fracture stresses of high pressure gas cylinders containing cracklike flaws. J Press Vessel Technol 129(4): 639–643. https://doi.org/10.1115/1.2767346
58. Rana MD, Selines RJ (1988) Structural integrity assurance of high-strength steel gas cylinders using fracture mechanics. Eng Fract Mech 30(6):877–894. https://doi.org/10.1016/0013-7944(88)90147-6
59. Rana MD, Smith JH, Tribolet RO (1997) Technical basis for flawed cylinder test specification to assure adequate fracture resistance of ISO high-strength steel cylinder. J Press Vessel Technol 119(4):475–480. https://doi.org/10.1115/1.2842332
60. Rothwell AB, Coote RI (2009) A critical review of assessment methods for axial planar surface flaws in pipe. In: Proceedings of the international conference on pipeline technology 2009, Ostend, Belgium.
61. Shannon RWE (1974) The failure behaviour of line pipe defects. Int J Press Vessel Pip 2:243–255. https://doi.org/10.1016/0308-0161(74)90006-4
62. Shih CF, Hutchinson JW (1975) Fully plastic solutions and large scale yielding estimates for plane stress crack problems. In: Report no. DEAP S-14. Harvard University, Cambridge
63. Staat M (2004) Plastic collapse analysis of longitudinally flawed pipes and vessels. Nucl Eng Des 234(1–3):25–43. https://doi.org/10.1016/j.nucengdes.2004.08.002
64. Yan J, Zhang S, Kariyawasam S, Pino M, Liu T (2018) Validate crack assessment models with in-service and hydrotest failures. In: Proceedings of international pipeline conference, IPC 2018–78251, Calgary. https://doi.org/10.1115/IPC2018-78251
65. Yan Z, Zhang S, Zhou W (2014) Model error assessment of burst capacity models for energy pipelines containing surface cracks. J Pressure Vessels Piping 120-121:80–92. https://doi.org/10.1016/j.ijpvp.2014.05.007
66. Yan J, Zhang S, Kariyawasam S, Lu D, Matchim T (2020) Reliability-based crack threat assessment and management. In: Proceedings of international pipeline conference, IPC 2020–9484. Online, Virtual. https://doi.org/10.1115/IPC2020-9484
67. Zadkarami M, Shahbazian M, Salahshoor K (2016) Pipeline leakage detection and isolation: an integrated approach of statistical and wavelet feature extraction with multi-layer perception neural network (MLPNN). J Loss Prev Process Ind 43:479–487. https://doi.org/10.1016/j.jlp.2016.06.018

68. Zadkarami M, Shahbazian M, Salahshoor K (2017) Pipeline leak diagnosis based on wavelet and statistical features using Dempster-Shafer classifier fusion technique. Process Saf Environ Prot 105:156–163. https://doi.org/10.1016/j.psep.2016.11.002
69. Zhou W, Xiang W, Cronin D (2016) Probability of rupture model for corroded pipelines. Int J Press Vessel Pip 147:1–11. https://doi.org/10.1016/j.ijpvp.2016.10.001

Publisher's Note